

Molar-ratio-dependent coordination assembly of organoiridium(III)-octatungstate complexes in aqueous solution

*Sugiarto, Jun Shinogi, and Masahiro Sadakane**

Department of Applied Chemistry, Graduate School of Advanced Science and Engineering,
Hiroshima University, 1-4-1 Kagamiyama, Higashi-Hiroshima 739-8527, Japan

ABSTRACT. We scrutinized the speciation of Cp*Ir-containing tungsten oxide clusters (Cp* is pentamethylcyclopentadienyl anion) in aqueous mixtures of [(Cp*IrCl)₂(μ-Cl)₂] and Na₂WO₄ in varying molar ratios. ¹H NMR spectroscopy revealed the formation of three distinct Cp*Ir-polyoxotungstate species in the reaction solution, and they were isolated as Na₄[(Cp*Ir)₂(μ-OH)₃]₂[(Cp*Ir)₂H₂W₈O₃₀] (**1**), [(Cp*Ir)₂(μ-OH)₃]₂[(Cp*Ir)₂{Cp*Ir(OH₂)₂}₂H₂W₈O₃₀] (**2**), and [(Cp*Ir)₂{Cp*Ir(OH₂)₂}₂{Cp*Ir(OH₂)₂}₂H₂W₈O₃₀](NO₃)₂ (**3**) from the mixtures in which iridium concentration is less than, equal to, and more than tungsten concentration, respectively. These results show octatungstate [H₂W₈O₃₀]¹⁰⁻ anion is the major polyoxotungstate species in the presence of {Cp*Ir}²⁺ cations, and it has high nucleophilicity enough to bind up to six {Cp*Ir}²⁺ cations on its surfaces producing a *cationic* Cp*Ir-octatungstate complex. The octatungstate anion was also generated from the reaction of [(Cp*IrCl)₂(μ-Cl)₂] and methylammonium paratungstate-

B, $(\text{CH}_3\text{NH}_3)_{10}[\text{H}_2\text{W}_{12}\text{O}_{42}]$, and was isolated as a methylamine-coordinated complex $(\text{CH}_3\text{NH}_3)_2[(\text{Cp}^*\text{Ir})_2\{\text{Cp}^*\text{Ir}(\text{NH}_2\text{CH}_3)\}_2\text{H}_2\text{W}_8\text{O}_{30}]$ (**4**), indicating $\{\text{Cp}^*\text{Ir}\}^{2+}$ cations function as a structure-directing agent that converts tungsten species into octatungstate anions in aqueous solution. In addition, coordination environment of $\{\text{Cp}^*\text{Ir}\}^{2+}$ can be further modified by coordination with pyridine forming $[\{\text{Cp}^*\text{Ir}(\text{NC}_5\text{H}_5)\}_2(\mu\text{-OH})_2][(\text{Cp}^*\text{Ir})_2\{\text{Cp}^*\text{Ir}(\text{NC}_5\text{H}_5)\}_2\text{H}_2\text{W}_8\text{O}_{30}]$ (**5**).

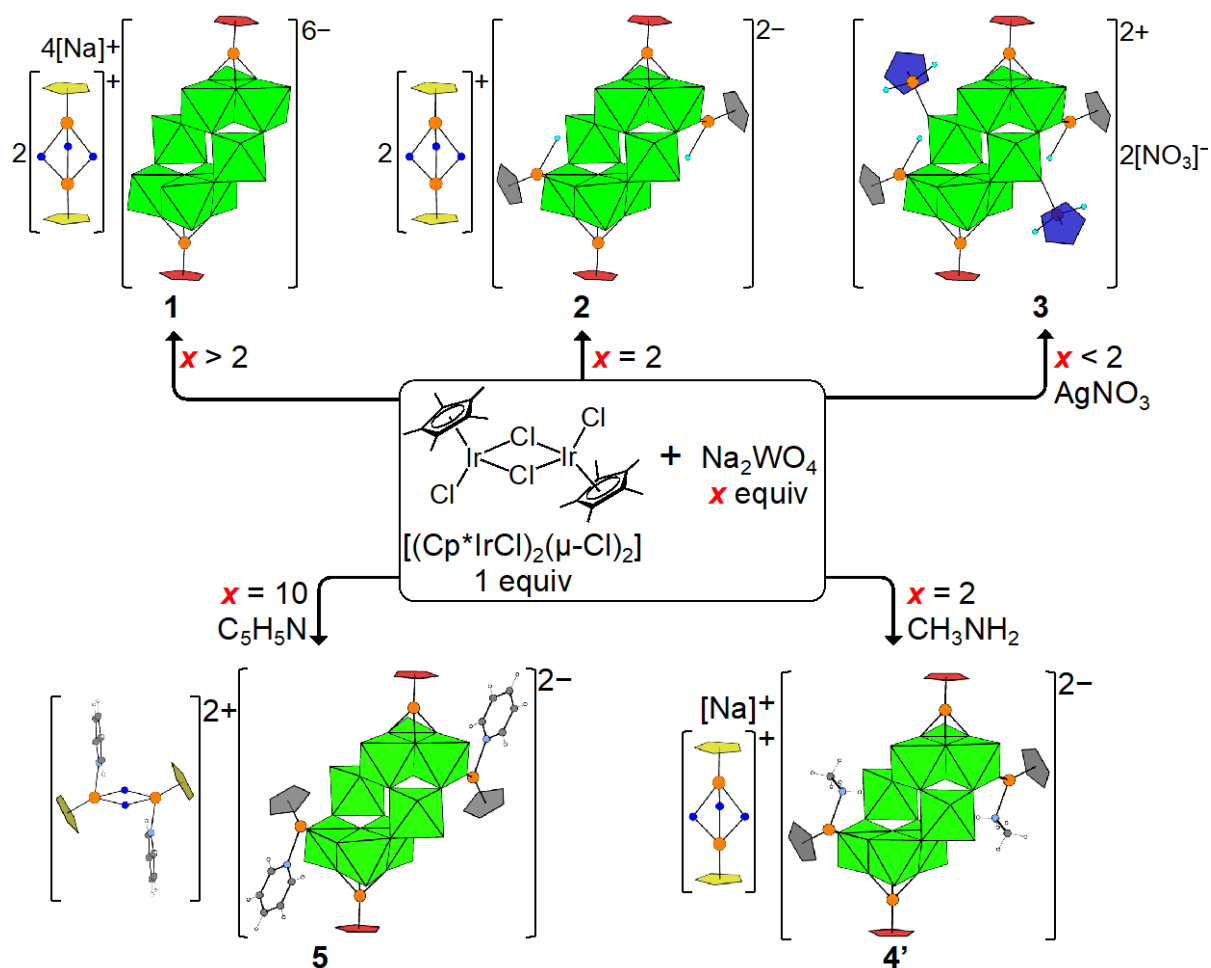
INTRODUCTION

Organometallic-polyoxometalate complexes are molecular metal oxide clusters of V, Nb, Ta, Mo, and W that contain additional peripheral organometallic fragments.¹⁻⁵ They have gained interest because their structures mimic interactions between organic substrates and oxide surfaces in heterogeneous catalysts⁶ and they are useful molecular precursors for the preparation of highly active solid catalysts.⁷⁻⁹ One characteristic of organometallic-polyoxometalate complexes is they have flexible organometallic–oxygen coordination bonds that facilitate structural transformation such as framework extension,¹⁰ isomerization,^{11, 12} intramolecular rearrangements,^{13, 14} and capping/decapping¹⁵ of the organometallic units, resulting in structural diversity. This framework flexibility is influenced by experimental conditions such as solvents, kinds of metal atoms and ligands,^{16, 17} and hence, exploring coordination chemistry of organometallic-polyoxometalate requires systematic approaches.

We are particularly interested in organoiridium(III)-containing polyoxotungstates^{6, 18} because they are relevant to water-oxidation catalysts based on Ir/WO₃ system.^{19, 20} Most known organoiridium(III)-polyoxotungstates contain $\{\text{Cp}^*\text{Ir}\}^{2+}$ (Cp* is pentamethylcyclopentadienyl anion, $\text{C}_5(\text{CH}_3)_5^-$) fragments; their structures and synthetic conditions are summarized in Table S1.

In 2018, Niu's group reported the first example of a Cp*Ir-polyoxotungstate complex formulated as $\text{H}_4[(\text{Cp}^*\text{Ir})_4\text{W}_8\text{O}_{32}] \cdot 17.33\text{H}_2\text{O}$ which was prepared by the reaction between $[(\text{Cp}^*\text{IrCl})_2(\mu\text{-Cl})_2]$ and Na_2WO_4 in a 1:4 molar ratio in water.²¹ It has an interesting structure featuring dangling $\{\text{Cp}^*\text{Ir}(\text{OH}_2)\}^{2+}$ units and is a useful precursor for electrodes active in hydrogen evolution reactions. Speciation of Cp*Ir-polyoxotungstate complexes in the reaction system, however, needs further clarification: the influence of $[(\text{Cp}^*\text{IrCl})_2(\mu\text{-Cl})_2]/\text{Na}_2\text{WO}_4$ molar ratios on structures is particularly worth attention. Abramov and co-workers have shown molar-ratio-dependent coordination assembly of Cp*Ir-polyoxoniobate and Cp*Ir-polyoxotantalate complexes.²² Moreover, our group found the reaction between $[\{(\text{C}_6\text{H}_6)\text{RuCl}\}_2(\mu\text{-Cl})_2]$ and $\text{K}_8[\text{SiW}_{10}\text{O}_{36}]$ in 1:2 and 1:4 molar ratios produces mono-grafted $[\{(\text{C}_6\text{H}_6)\text{Ru}\}\text{SiW}_{10}\text{O}_{36}]^{6-}$ and di-grafted $[\{(\text{C}_6\text{H}_6)\text{Ru}\}_2\{(\text{C}_6\text{H}_6)\text{Ru}(\text{OH}_2)\}_2\text{SiW}_{10}\text{O}_{36}]^{4-}$ clusters, respectively.^{23, 24}

Herein, we report on a systematic study on the speciation of Cp*Ir-polyoxotungstate complexes in aqueous mixtures of $[(\text{Cp}^*\text{IrCl})_2(\mu\text{-Cl})_2]$ and Na_2WO_4 . Five compounds— $\text{Na}_4[(\text{Cp}^*\text{Ir})_2(\mu\text{-OH})_3]_2[(\text{Cp}^*\text{Ir})_2\text{H}_2\text{W}_8\text{O}_{30}]$ (**1**), $[(\text{Cp}^*\text{Ir})_2(\mu\text{-OH})_3]_2[(\text{Cp}^*\text{Ir})_2\{\text{Cp}^*\text{Ir}(\text{OH}_2)\}_2\text{H}_2\text{W}_8\text{O}_{30}]$ (**2**), $[(\text{Cp}^*\text{Ir})_2\{\text{Cp}^*\text{Ir}(\text{OH}_2)\}_2\{\text{Cp}^*\text{Ir}(\text{OH}_2)_2\}_2\text{H}_2\text{W}_8\text{O}_{30}](\text{NO}_3)_2$ (**3**), $(\text{CH}_3\text{NH}_3)_2[(\text{Cp}^*\text{Ir})_2\{\text{Cp}^*\text{Ir}(\text{NH}_2\text{CH}_3)\}_2\text{H}_2\text{W}_8\text{O}_{30}]$ (**4**), and $[\{\text{Cp}^*\text{Ir}(\text{NC}_5\text{H}_5)\}_2(\mu\text{-OH})_2][(\text{Cp}^*\text{Ir})_2\{\text{Cp}^*\text{Ir}(\text{NC}_5\text{H}_5)\}_2\text{H}_2\text{W}_8\text{O}_{30}]$ (**5**)—were isolated (Scheme 1), and their solid-state structures were determined using single-crystal X-ray diffraction. Coordination assembly of **1–3** in the reaction mixtures was monitored using ^1H NMR spectroscopy.



Scheme 1. Simplified illustration of synthetic conditions and structures of Cp*Ir-octatungstate complexes in this work. Octatungstate is represented by green polyhedra, whereas Cp* rings are shown as pentagons: yellow for Cp* of the counter cations, red for Cp*Ir units, gray for {Cp*Ir(aquo/amine)} units, and blue for {Cp*Ir(OH₂)₂} units pentagons. Orange, deep blue, light blue, cyan, and white circles are Ir, OH, N, OH₂, and H respectively.

EXPERIMENTAL SECTION

Materials and analytical methods. Chemicals were purchased and used as received. Homemade distilled water was used (Elix, Essential). Fourier Transform Infrared Spectroscopy (FTIR) spectra were collected using a KBr disc on a ThermoFisher Scientific Nicolet 6700 FTIR

spectrometer. ^1H NMR spectra were recorded on a Variant system 500 (500 MHz; H resonance frequency = 499.827 MHz) spectrometer at ambient temperature and chemical shifts were referred to the solvent residual signal. Thermogravimetric (TG) analysis was carried out using Hitachi SII TG/DTA7300 analyzer with a heating rate of 10 °C per minute under a constant airflow (100 mL/minute); all compounds easily lose their water solvates, and their thermograms are given in Figure S1. Total elemental (non-oxygen) analyses for compounds **1**, **2**, and **4** were carried out by Mikroanalytisches Labor Pascher (Remagen, Germany), whereas CHN analyses of **3** and **5** were performed by the Division of Instrumental Analysis at Okayama University.

Synthesis of $\text{Na}_4[(\text{Cp}^*\text{Ir})_2(\mu\text{-OH})_3]_2[(\text{Cp}^*\text{Ir})_2\text{H}_2\text{W}_8\text{O}_{30}]$ (1** = $\text{Na}_4[(\text{Cp}^*\text{Ir})_2(\mu\text{-OH})_3]_2 \cdot \mathbf{1a}$, $\mathbf{1a}$ = $[(\text{Cp}^*\text{Ir})_2\text{H}_2\text{W}_8\text{O}_{30}]^{6-}$). A mixture of $[(\text{Cp}^*\text{IrCl})_2(\mu\text{-Cl})_2]$ (40.0 mg; 0.05 mmol) and $\text{Na}_2\text{WO}_4 \cdot 2\text{H}_2\text{O}$ (165.6 mg; 0.5 mmol) in water (2.0 mL) in a sealed reaction tube was heated in a metal bath at 80 °C for 30 minutes to give a clear greenish yellow solution (pH 8.0). The solution was cooled down to room temperature, filtered, and set for crystallization in an uncapped vial at 27°C. Green-yellow rectangular crystals appeared overnight and were harvested after one week. The crystals were rinsed several times with water and dried in the air. Yield = 54.1 mg (69% based on Ir). Elem. Anal. Calcd for $\text{Na}_{4.1}[(\text{Cp}^*\text{Ir})_2(\mu\text{-OH})_3]_{1.9}[(\text{Cp}^*\text{Ir})_2\text{H}_2\text{W}_8\text{O}_{30}] \cdot 37\text{H}_2\text{O}$: C, 14.79; H, 3.62; Ir, 23.67; Na, 2.00; W, 31.22. Found: C, 14.95; H, 3.26; Ir, 23.3; Na, 1.89; W, 31.4. TG up to 210 °C found a 12.01% decrease in weight corresponding to the loss of 31 water molecules (calcd 11.96%). ^1H NMR (in 1M $\text{KNO}_3/\text{D}_2\text{O}$, δ/ppm): 1.59 (s, 30H, **1a**), 1.53 (s, 60H, $[(\text{Cp}^*\text{Ir})_2(\mu\text{-OH})_3]^+$). FTIR (KBr disc, v/cm^{-1}): 1477, 1456, 1387, 1076, 1034, 926, 897, 874, 823, 770.**

Crystal obtained from a 1:10 $[(\text{Cp}^*\text{IrCl})_2(\mu\text{-Cl})_2]/\text{Na}_2\text{WO}_4$ mixture was often twinned or cracked. Diffraction-quality crystal of **1** could be obtained from a 1:6 $[(\text{Cp}^*\text{IrCl})_2(\mu\text{-Cl})_2]/\text{Na}_2\text{WO}_4$ mixture as follows: a mixture of $[(\text{Cp}^*\text{IrCl})_2(\mu\text{-Cl})_2]$ (10.0 mg; 0.0125 mmol) and $\text{Na}_2\text{WO}_4 \cdot 2\text{H}_2\text{O}$ (24.9

mg; 0.08 mmol) in water (0.5 mL) in a sealed reaction tube was heated in a metal bath at 80 °C for 15 minutes. Yellow crystals were deposited after standing overnight in a capped container.

Synthesis of $[(\text{Cp}^*\text{Ir})_2(\mu\text{-OH})_3]_2[(\text{Cp}^*\text{Ir})_2\{\text{Cp}^*\text{Ir}(\text{OH}_2)\}_2\text{H}_2\text{W}_8\text{O}_{30}]$ (2** = $[(\text{Cp}^*\text{Ir})_2(\mu\text{-OH})_3]_2\cdot\mathbf{2a}$, $\mathbf{2a} = [(\text{Cp}^*\text{Ir})_2\{\text{Cp}^*\text{Ir}(\text{OH}_2)\}_2\text{H}_2\text{W}_8\text{O}_{30}]^{2-}$).** A mixture of $[(\text{Cp}^*\text{IrCl})_2(\mu\text{-Cl})_2]$ (40.0 mg; 0.05 mmol) and $\text{Na}_2\text{WO}_4\cdot 2\text{H}_2\text{O}$ (33.0 mg; 0.1 mmol) in water (2.0 mL) in a sealed reaction tube was heated in a metal bath at 80 °C for 30 minutes. The solution was cooled down to room temperature, and a few unreacted $[(\text{Cp}^*\text{IrCl})_2(\mu\text{-Cl})_2]$ solid was filtered out. The clear yellow filtrate (pH 5.72) was allowed to evaporate in a loosely capped vial at 27°C. Large yellow crystals formed after 1-2 days and were harvested after one week. The crystals were rinsed with a few drops of water, and if necessary, a few drops of dichloromethane to remove any orange solids of $[(\text{Cp}^*\text{IrCl})_2(\mu\text{-Cl})_2]$. Yield = 40.3 mg (59% based on Ir). Elem. Anal. Calcd for $[(\text{Cp}^*\text{Ir})_2(\mu\text{-OH})_3]_2[(\text{Cp}^*\text{Ir})_2\{\text{Cp}^*\text{Ir}(\text{OH}_2)\}_2\text{H}_2\text{W}_8\text{O}_{30}]\cdot 42\text{H}_2\text{O}$: C, 17.57; H, 3.99; Ir, 28.13; W, 26.9. Found: C, 17.77; H, 3.87; Ir, 27.7; W, 27.1. TG up to 150 °C found a 13.26% decrease in weight due to the loss of 40 water molecules (calcd 13.36%). ^1H NMR (in 1:29 $\text{CD}_3\text{OH}/\text{D}_2\text{O}$, δ/ppm): 1.52 (s, 30H, **2a**), 1.50 (s, 30H, **2a**), 1.44 (s, 60H, $[(\text{Cp}^*\text{Ir})_2(\mu\text{-OH})_3]^+$). FTIR (KBr disc, v/cm^{-1}): 1477, 1456, 1387, 1080, 1032, 924, 895, 872, 824, 754.

Synthesis of $[(\text{Cp}^*\text{Ir})_2\{\text{Cp}^*\text{Ir}(\text{OH}_2)\}_2\{\text{Cp}^*\text{Ir}(\text{OH}_2)_2\}_2\text{H}_2\text{W}_8\text{O}_{30}](\text{NO}_3)_2$ (3** = $\mathbf{3a}\cdot(\text{NO}_3)_2$, $\mathbf{3a} = [(\text{Cp}^*\text{Ir})_2\{\text{Cp}^*\text{Ir}(\text{OH}_2)\}_2\{\text{Cp}^*\text{Ir}(\text{OH}_2)_2\}_2\text{H}_2\text{W}_8\text{O}_{30}]^{2+}$).** $[(\text{Cp}^*\text{IrCl})_2(\mu\text{-Cl})_2]$ (40.0 mg; 0.05 mmol) was dissolved in 0.1 M aqueous AgNO_3 solution (2.0 mL; 0.2 mmol) under vigorous stirring for 30 minutes in dark and precipitated AgCl was discarded by filtration. To the clear green-yellow filtrate was added solid $\text{Na}_2\text{WO}_4\cdot 2\text{H}_2\text{O}$ (16.5 mg; 0.05 mmol), resulting in the precipitation of a yellow solid. The mixture (pH = 2.33) was finely filtered and solid NaNO_3 (340.6 mg; 4.0 mmol) was added. Greenish-yellow crystals started to deposit immediately and were

harvested after 1 day. Yield = 15.0 mg, 54% based on W. Elem. Anal. Calcd for $[(\text{Cp}^*\text{Ir})_2\{\text{Cp}^*\text{Ir}(\text{OH}_2)\}_2\{\text{Cp}^*\text{Ir}(\text{OH}_2)_2\}_2\text{H}_2\text{W}_8\text{O}_{30}](\text{NO}_3)_2 \cdot 14\text{H}_2\text{O}$: C, 16.37; H, 3.03; N, 0.64. Found: C, 16.32; H, 2.88; N, 0.65. TG analysis up to 150 °C found a 9.74% decrease in weight corresponding to the loss of 24H₂O (calcd 9.67%). ¹H NMR (in CD₃CN, δ/ppm): 1.85 (s, 30H, **3a**), 1.75 (s, 30H, **3a**), and 1.69 (s, 30H, **3a**). Note that minor singlets at 1.82, 1.77, 1.72–1.70 ppm were presumably attributed to acetonitrile-coordinated complexes. FTIR (KBr disc, ν/cm⁻¹): 1477, 1452, 1385, 1080, 1032, 930, 877, 866, 795, 764.

On prolonged standing of the reaction mixture, large pale green crystals of $[(\text{Cp}^*\text{Ir})_2(\mu\text{-OH})_3](\text{NO}_3) \cdot 6\text{H}_2\text{O}$ were deposited (see Figure S2 for structure and crystallographic parameters).

Synthesis of $(\text{CH}_3\text{NH}_3)_2[(\text{Cp}^*\text{Ir})_2\{\text{Cp}^*\text{Ir}(\text{NH}_2\text{CH}_3)\}_2\text{H}_2\text{W}_8\text{O}_{30}]$ (4** = $(\text{CH}_3\text{NH}_3)_2 \cdot \mathbf{4a}$, **4a** = $[(\text{Cp}^*\text{Ir})_2\{\text{Cp}^*\text{Ir}(\text{NH}_2\text{CH}_3)\}_2\text{H}_2\text{W}_8\text{O}_{30}]^{2-}$).** A mixture of $[(\text{Cp}^*\text{IrCl})_2(\mu\text{-Cl})_2]$ (20.0 mg; 0.025 mmol) and $(\text{CH}_3\text{NH}_3)_{10}[\text{H}_2\text{W}_{12}\text{O}_{42}]$ (160.4 mg; 0.05 mmol) in water (1.5 mL) in a sealed reaction tube was heated in a metal bath at 80 °C for an hour. Any unreacted solids were removed by filtration, and the clear solution (pH 4.82) was allowed to evaporate in a glass vial. After standing for one week, deposited yellow crystals were harvested and washed with dichloromethane to remove $[(\text{Cp}^*\text{Ir})_2(\mu\text{-OH})_3]^+$ contaminants. Yield = 16 mg (34% based on Ir). Elem. Anal. Calcd for $(\text{CH}_3\text{NH}_3)_2[(\text{Cp}^*\text{Ir})_2\{\text{Cp}^*\text{Ir}(\text{NH}_2\text{CH}_3)\}_2\text{H}_2\text{W}_8\text{O}_{30}] \cdot 20\text{H}_2\text{O}$: C, 14.10; H, 3.34; Ir, 20.51; N, 1.49; W, 39.22. Found: C, 13.78; H, 3.09; Ir, 19.90; N, 1.27; W, 39.70. TG analysis up to 300 °C found a 7.39% decrease in weight corresponding to the loss of eight H₂O, two CH₃NH₂, and two CH₃NH₃⁺ (calcd 7.39%). ¹H NMR (in D₂O, δ/ppm): 2.75 (s, 6H, Ir-coordinating CH₃NH₂ ligand), 2.45 (s, 6H, CH₃NH₃⁺), 1.57 (s, 30H, **4a**), and 1.53 (s, 30H, **4a**). FTIR (KBr disc, ν/cm⁻¹): 1456, 1385, 1078, 1034, 928, 879, 820, 748.

Crystal of **4** was twinned; single-crystal was prepared as follows: a mixture of $[(\text{Cp}^*\text{IrCl})_2(\mu\text{-Cl})_2]$ (20.0 mg; 0.025 mmol) and $\text{Na}_2\text{WO}_4 \cdot 2\text{H}_2\text{O}$ (16.5 mg; 0.05 mmol) in water (1.0 mL) in a sealed glass vial was heated in a metal bath at 80 °C for 30 minutes. The solution was cooled down to room temperature and any unreacted $[(\text{Cp}^*\text{IrCl})_2(\mu\text{-Cl})_2]$ was discarded by filtration. The clear filtrate was alkalinized to pH 7.5–8.0 by the careful addition of an aqueous methylamine solution (40%). The resulting yellow solution was left overnight in an open vial to deposit yellow blocks of $\text{Na}[(\text{Cp}^*\text{Ir})_2(\mu\text{-OH})_3]\text{-4a} \cdot 36\text{H}_2\text{O}$ (**4'**).

Synthesis of $[(\text{Cp}^*\text{Ir}(\text{NC}_5\text{H}_5))_2(\mu\text{-OH})_2][(\text{Cp}^*\text{Ir})_2\{\text{Cp}^*\text{Ir}(\text{NC}_5\text{H}_5)\}_2\text{H}_2\text{W}_8\text{O}_{30}]$ (5** = $[(\text{Cp}^*\text{Ir}(\text{NC}_5\text{H}_5))_2(\mu\text{-OH})_2] \cdot \mathbf{5a}$, $\mathbf{5a} = [(\text{Cp}^*\text{Ir})_2\{\text{Cp}^*\text{Ir}(\text{NC}_5\text{H}_5)\}_2\text{H}_2\text{W}_8\text{O}_{30}]^{2-}$).** $\text{Na}_2\text{WO}_4 \cdot 2\text{H}_2\text{O}$ (66.1 mg; 0.20 mmol) was dissolved in water (1.0 mL) and pyridine (0.2 mL; 2.48 mmol) was added. To the slightly turbid solution was added $[(\text{Cp}^*\text{IrCl})_2(\mu\text{-Cl})_2]$ (16.1 mg; 0.02 mmol), and the mixture was heated in a metal bath (80 °C) for 30 minutes and was finely filtered at room temperature to give clear yellow solution (pH 8.50). Standing the solution at room temperature for one week gave yellow crystals. Yield = 11.6 mg (39% based on Ir). Elem. Anal. Calcd for $[(\text{Cp}^*\text{Ir}(\text{NC}_5\text{H}_5))_2(\mu\text{-OH})_2][(\text{Cp}^*\text{Ir})_2\{\text{Cp}^*\text{Ir}(\text{NC}_5\text{H}_5)\}_2\text{H}_2\text{W}_8\text{O}_{30}] \cdot 7\text{H}_2\text{O}$: C, 21.87; H, 3.18; N, 1.28. Found: C, 22.19; H, 3.18; N, 1.67. TG analysis up to 74 °C found a 3.06% decrease in weight corresponding to the loss of seven H_2O (calcd 2.87%). FTIR (KBr disc, ν/cm^{-1}): 1448, 1379, 1070, 1032, 925, 881, 814, 748.

X-ray crystallography. Single crystal suitable for X-ray diffraction was suspended in mineral oil and mounted on a goniometer head under a nitrogen stream. Intensity data were collected at –150 °C (except for **4**, at –183 °C) on a Bruker SMART APEXII diffractometer equipped with a CCD detector and a Mo K α radiation ($\lambda = 0.71073 \text{ \AA}$) source monochromated by layered confocal mirrors. Data reduction, integration, and scaling were performed on a Bruker APEX3 suite.²⁵

Intensities were corrected against absorption using SADABS.²⁵ Initial structure was solved using SHEXL²⁶ program and subsequently refined using SHELXL²⁷ running on a ShelXle²⁸ user interface. Some disordered crystallization water was removed using routine Platon SQUEEZE.²⁹ All non-hydrogen atoms were refined anisotropically. Hydrogen atoms of Cp* ligands were generated on the calculated positions using a riding model. Crystal of **4** was twinned (R_1 for $I > 2\sigma(I)$ = 16.08%; Platon TwinRotMat program found a twin law $-1\ 0\ 0\ 0\ 0\ -1\ 0\ 0.786\ 0\ 1$ with BASF 0.43 and a 6.09% drop in R_1 value); indexing and unit cell determination was performed using CELL_NOW (Bruker APEX3), whereas scaling and absorption correction was done using TWINABS, generating detwinned (HKLF4) and twinned (HKLF5, two domains) reflection data. The final structure was refined against HKLF5 which significantly reduced R_1 for $I > 2\sigma(I)$ to 4.31%. Detailed crystallographic parameters are summarized in Table S2 and are available free of charge at the Cambridge Crystallography Data Centre by quoting CCDC numbers 2218945–9 and 2226842 (twinned data set of **4**).

Bond Valence Sum (BVS) calculation. The BVS values were calculated by the expression (equation 1) for the variation of the length r_{ij} of a bond between two atoms i and j in an observed crystal with valence V_i

$$V_i = \sum_j \exp\left(\frac{r'_0 - r_{ij}}{B}\right) \quad (1)$$

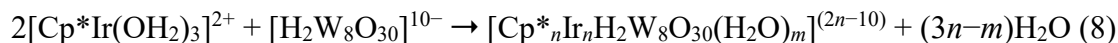
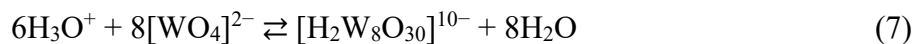
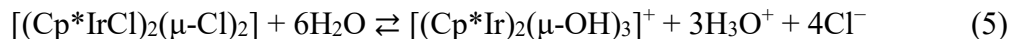
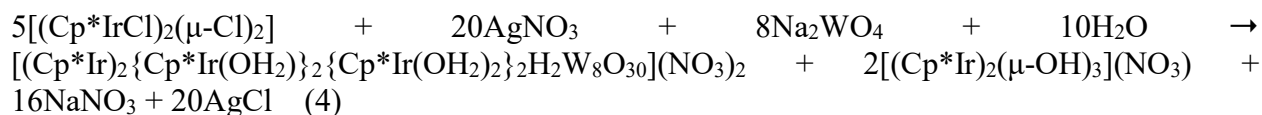
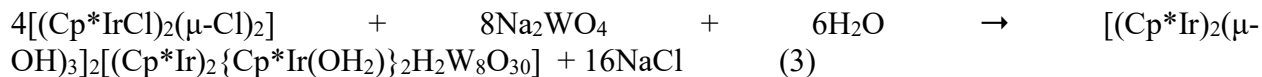
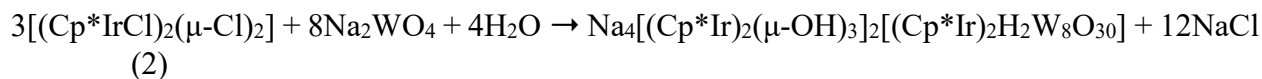
where B is a constant equal to 0.37 Å for W and 0.414 for Ir, and r'_0 is a bond valence parameter for a given atom pair; $r'_0 = 1.906$ Å for W(VI)–O pair and $r'_0 = 1.755$ Å for Ir(III)–O pair³⁰ were used to calculate BVS of tungsten and oxygen atoms in **1–5**. Results of BVS calculation are tabulated in Table S3.

RESULTS AND DISCUSSION

Syntheses. The reaction between $[(\text{Cp}^*\text{IrCl})_2(\mu\text{-Cl})_2]$ and Na_2WO_4 in aqueous solution produced three kinds of Cp^*Ir -octatungstate complexes, $[(\text{Cp}^*\text{Ir})_2\text{H}_2\text{W}_8\text{O}_{30}]^{6-}$ (**1a**), $[(\text{Cp}^*\text{Ir})_2\{\text{Cp}^*\text{Ir}(\text{OH}_2)\}_2\text{H}_2\text{W}_8\text{O}_{30}]^{2-}$ (**2a**), and $[(\text{Cp}^*\text{Ir})_2\{\text{Cp}^*\text{Ir}(\text{OH}_2)\}_2\{\text{Cp}^*\text{Ir}(\text{OH}_2)_2\}_2\text{H}_2\text{W}_8\text{O}_{30}]^{2+}$ (**3a**), and their formation was controllable by adjusting the molar ratio of $[(\text{Cp}^*\text{IrCl})_2(\mu\text{-Cl})_2]$ to Na_2WO_4 (Scheme 1). The anionic complexes **1a** and **2a** formed in $[(\text{Cp}^*\text{IrCl})_2(\mu\text{-Cl})_2]/\text{Na}_2\text{WO}_4$ mixtures in which total iridium concentration is less than (for example, $[(\text{Cp}^*\text{IrCl})_2(\mu\text{-Cl})_2]:\text{Na}_2\text{WO}_4$ molar ratios = 1:10, 1:8, 1:6, or 1:4) and equal to ($[(\text{Cp}^*\text{IrCl})_2(\mu\text{-Cl})_2]:\text{Na}_2\text{WO}_4$ molar ratio = 1:2) tungsten concentration, respectively; they could be crystallized directly from the reaction mixture as $\text{Na}_4[(\text{Cp}^*\text{Ir})_2(\mu\text{-OH})_3]_2[(\text{Cp}^*\text{Ir})_2\text{H}_2\text{W}_8\text{O}_{30}]$ (**1**) and $[(\text{Cp}^*\text{Ir})_2(\mu\text{-OH})_3]_2[(\text{Cp}^*\text{Ir})_2\{\text{Cp}^*\text{Ir}(\text{OH}_2)\}_2\text{H}_2\text{W}_8\text{O}_{30}]$ (**2**). On the other hand, the cationic complex **3a** that was generated in a 1:1 $[(\text{Cp}^*\text{IrCl})_2(\mu\text{-Cl})_2]/\text{Na}_2\text{WO}_4$ mixture could not be isolated from the mixture. This is because $[(\text{Cp}^*\text{IrCl})_2(\mu\text{-Cl})_2]$ constantly precipitates from the mixture, reducing total iridium concentration relative to tungsten concentration. To isolate **3a**, two conditions are required: (i) $\{\text{Cp}^*\text{Ir}\}^{2+}:\text{WO}_4^{2-}$ molar ratio must be maintained at 2:1; this is achieved by dissolving 1 equivalent of $[(\text{Cp}^*\text{IrCl})_2(\mu\text{-Cl})_2]$ in 4 equivalents of aqueous silver nitrate to generate 2 equivalents of $[\text{Cp}^*\text{Ir}(\text{OH}_2)_3]^{2+}$ and followed by the addition of 1 equivalent of Na_2WO_4 , and (ii) large excess of sodium nitrate must be added to promote crystallization of the cationic cluster as $[(\text{Cp}^*\text{Ir})_2\{\text{Cp}^*\text{Ir}(\text{OH}_2)\}_2\{\text{Cp}^*\text{Ir}(\text{OH}_2)_2\}_2\text{H}_2\text{W}_8\text{O}_{30}](\text{NO}_3)_2$ (**3**). Reactions with higher iridium concentration—for example by mixing $[(\text{Cp}^*\text{IrCl})_2(\mu\text{-Cl})_2]$, AgNO_3 , and Na_2WO_4 in a 1:4:0.5 molar ratio—produced no new compounds, but **3** was crystallized. This is because, presumably, coordination of $\{\text{Cp}^*\text{Ir}\}^{2+}$ to **3a** is electrostatically unfavorable due to cation-cation repulsion. As such, **1a**, **2a**, and **3a** are the three major species isolable from aqueous $[(\text{Cp}^*\text{IrCl})_2(\mu\text{-Cl})_2]/\text{Na}_2\text{WO}_4$

mixtures in a wide range of reactant compositions. Compounds **1–3** display similar infrared absorption patterns arising from Cp* and octatungstate (see Figure S3).

Formation of **1–3** is stoichiometrically expressed by equations 2–4. In the reaction system, [(Cp*IrCl)₂(μ-Cl)₂] functions as a source of protons and [(Cp*Ir)₂(μ-OH)₃]⁺ counter cations (equation 5); structure of [(Cp*Ir)₂(μ-OH)₃](CH₃COO) has been determined,³¹ and we also determined the crystal structure of [(Cp*Ir)₂(μ-OH)₃](NO₃)·6H₂O (Figure S2). The released protons are consumed (i) by [(Cp*Ir)₂(μ-OH)₃]⁺ to form a minor amount of [Cp*Ir(OH₂)₃]²⁺ cations (equation 6) and (ii) by tungstate anions (a weak base) to form octatungstate anions via acid condensation reactions (equation 7). Finally, ligand substitution reactions between [Cp*Ir(OH₂)₃]²⁺ and [H₂W₈O₃₀]¹⁰⁻ afford Cp*Ir-octatungstate complexes containing two, four, or six {Cp*Ir}²⁺ fragments (equation 8) that are detected in the reaction mixtures by ¹H NMR spectroscopy (see under speciation section).



In addition to the molar ratio, the pH of the [(Cp*IrCl)₂(μ-Cl)₂]/Na₂WO₄ mixtures also influences complex formation. For example, when a 1:10 [(Cp*IrCl)₂(μ-Cl)₂]/Na₂WO₄ mixture

(initial pH around 8) was acidified by aqueous perchloric acid to pH 4.5–4.7, **1** could not be obtained but **2a** was crystallized as a sodium salt $\text{Na}_2[(\text{Cp}^*\text{Ir})_2\{\text{Cp}^*\text{Ir}(\text{OH}_2)\}_2\text{H}_2\text{W}_8\text{O}_{30}]\cdot 26\text{H}_2\text{O}$ (Figure S4). In other words, the anionic complex **2a** can be isolated from mild acidic mixtures (pH around 5–6) regardless of $[(\text{Cp}^*\text{IrCl})_2(\mu\text{-Cl})_2]/\text{Na}_2\text{WO}_4$ molar ratios. On the other hand, adjusting the pH of a 1:2 $[(\text{Cp}^*\text{IrCl})_2(\mu\text{-Cl})_2]/\text{Na}_2\text{WO}_4$ mixture (initial pH around 6) by aqueous sodium hydroxide to pH 8 did not produce **1** but $[(\text{Cp}^*\text{Ir})_2(\mu\text{-OH})_3](\text{OH})$ was isolated, therefore, isolation of **1** requires precise control over $[(\text{Cp}^*\text{IrCl})_2(\mu\text{-Cl})_2]/\text{Na}_2\text{WO}_4$ molar ratios.

X-ray crystal structures. Compound **1** crystallizes in the triclinic system space group $P\bar{1}$, and the structure of anion **1a** is shown in Figure 1a. It comprises an octatungstate $[\text{H}_2\text{W}_8\text{O}_{30}]^{10-}$ anion that is coordinated by two peripheral $\{\text{Cp}^*\text{Ir}\}^{2+}$ units. The octatungstate anion (Figure 1b) is similar to that reported by Proust⁴ and Niu³² and is described as two incomplete-cubane-shaped $\{\text{W}_3\text{O}_{12}(\mu_3\text{-OH})\}^{7-}$ fragments linked by two *cis*- $\{\text{WO}_2\}^{2+}$, forming a sandwich-like structure. On each $\{\text{W}_3\text{O}_{12}(\mu_3\text{-OH})\}^{7-}$ fragment the oxygen atom (O14) that bridges three tungsten atoms is protonated, as confirmed by BVS calculations (BVS O14 = 1.16; see Table S3 for BVS values of all tungsten and oxygen atoms). The two $\{\text{W}_3\text{O}_{12}(\mu_3\text{-OH})\}^{7-}$ fragments interact with one another through intramolecular $\mu_3\text{-OH}\cdots\text{O}$ hydrogen bonds with an average donor-acceptor distance of 2.875 Å. The incomplete-cubane site on each $\{\text{W}_3\text{O}_{12}(\mu_3\text{-OH})\}^{7-}$ fragment is capped by a $\{\text{Cp}^*\text{Ir}\}^{2+}$ cation, resulting in a W_3IrO_4 cube; the Ir(III) centers adopt a pseudo-octahedral piano-stool geometry common for half-sandwich organometallic complexes, and the average Ir–O bond distance is 2.11 Å. The overall symmetry of **1a** is C_{2h} so that the two $\{\text{Cp}^*\text{Ir}\}^{2+}$ units are symmetrically equivalent. The –6 charge of **1a** is counter-balanced by four sodium and two $[(\text{Cp}^*\text{Ir})_2(\mu\text{-OH})_3]^+$ cations, as confirmed by X-ray diffraction and elemental analysis results. The structure of $[(\text{Cp}^*\text{Ir})_2(\mu\text{-OH})_3]^+$ cations as their acetate salt has been reported;³¹ we also solved the

crystal structure of their nitrate salt (see Figure S2). In the crystal packing, **1a** is linked by sodium cations into a chain-like structure that propagates along *a* direction (Figure 1c).

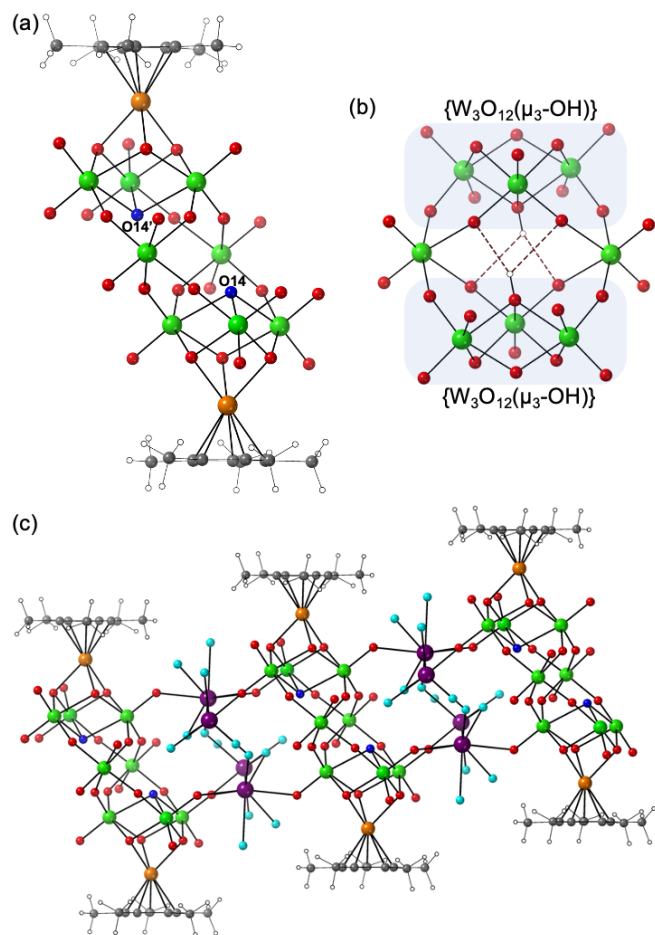


Figure 1. Ball-and-stick models of (a) **1a**, (b) a front view of octatungstate $[H_2W_8O_{30}]^{10-}$ anion with intramolecular hydrogen bonds showed as dashed red lines, and (c) sodium-linked **1a** in the crystal packing. Color scheme: green, W; orange, Ir; purple, Na; red, O; blue, protonated O (OH^-); cyan, O of aquo ligands; gray, C; white, H.

Compound **2** crystallizes in the monoclinic system space group $C2/m$ and is composed of two $[(Cp^*Ir)_2(\mu-OH)_3]^+$ counter cations and an anionic **2a** cluster (Figure 2a). The structure of **2a** can be built from **1a** by attaching on each $\{W_3O_{12}(\mu_3-OH)\}^{7-}$ fragment a mono-aquo $\{Cp^*Ir(OH_2)\}^{2+}$

units through coordination with vicinal $\{W=O\}$ groups (see inset, Figure 2a); the Ir–OW bond distance is 2.08 Å. The W=OIr bond distance is 1.79 Å, indicating a significant double bond character (compared to the non-coordinating W=O bond distance at 1.74 Å) is preserved on ligating. The Ir(III)–OH₂ bond distance is 2.157 Å³³ and the BVS of O10 is 0.38, further supporting the assignment of aquo ligand is correct. As we mentioned in Introduction, Niu and co-workers reported a similar Cp*Ir-octatungstate H₄[(Cp*Ir)₄W₈O₃₂]·17.33H₂O;²¹ based on the deposited crystal structure, the formula can be rewritten as [(Cp*Ir)₂{Cp*Ir(OH₂)₂W₈O₃₀}⁴⁻ in which the octatungstate core is not protonated. In contrast to their structure, **2a** contains two protons located on O3 and its symmetrically equivalent O3' (BVS = 1.22) and hence bears a –2 charge.

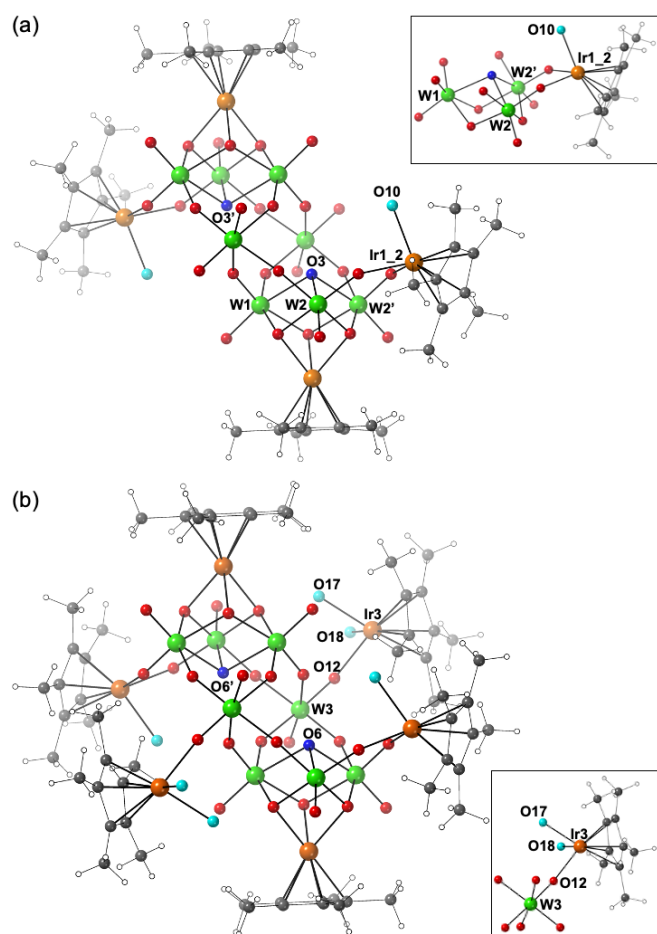


Figure 2. Ball-and-stick models of (a) **2a** and (b) **3a**. Cp* ligands in **2a** are disordered into two parts, and only one part is shown. Insets are enlarged views of the coordination environment around respective iridium centers. Color scheme: green, W; orange, Ir; red, O; blue, protonated O (OH⁺); cyan, O of aquo ligands; gray, C; white, H.

While **1** and **2** contain *anionic* Cp*Ir-octatungstate clusters, **3** is a nitrate salt of *cationic* Cp*Ir-octatungstate complex **3a**. The structure of **3a** (Figure 2b) can be derived from **2a** by connecting a diaquo {Cp*Ir(OH₂)₂}²⁺ fragment to each *cis*-{WO₂}²⁺ unit via one of the terminal oxygen atoms (O12). Ir3–O17 and Ir3–O18 bond distances are 2.18 and 2.16 Å, and BVS values of O17 and O18 are 0.36 and 0.38, confirming O17 and O18 are aquo ligands. The octatungstate anion in **3a** is also doubly protonated (at O6 and its symmetrically equivalent O6', BVS = 1.23); the high crystal quality of **3** allowed us to locate the protons in the difference map. The negative charge (–10) of octatungstate is surpassed by coordination with six {Cp*Ir}²⁺ cations (total positive charge = +12) so that **3a** bears a net +2 charge which is, as far as we know, the first example of cationic organoiridium-containing polyoxometalates. In the crystal packing (Figure 3), nitrate anion is sandwiched between {Cp*Ir(OH₂)₂}²⁺ and {Cp*Ir(OH₂)₂}²⁺ fragments and forms unconventional anion- π interactions³⁴⁻³⁷ in which nitrate's plane is pseudo-parallel relative to the Cp* rings; the distances from nitrate's oxygen atoms to the center of Cp* rings are in a range of 3.33–4.05 Å.

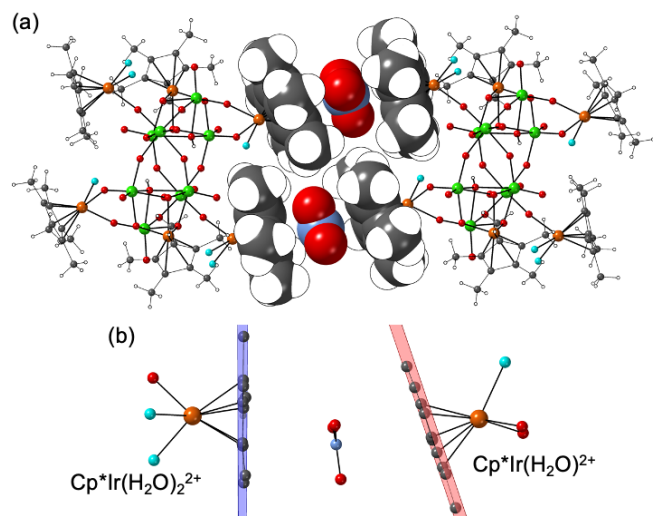


Figure 3. (a) A segment of the crystal packing of **3** showing π -nitrate interactions. Nitrate anions and Cp* ligands involved in π -nitrate interactions are displayed in the space-filling model. (b) Relative orientation of nitrate anion with respect to Cp* rings of $\{\text{Cp}^*\text{Ir}(\text{OH}_2)_2\}^{2+}$ (blue plane) and $\{\text{Cp}^*\text{Ir}(\text{OH}_2)\}^{2+}$ (red plane). Color scheme: green, W; orange, Ir; red, O; blue, protonated O (OH^-); cyan, O of aquo ligands; gray, C; white, H.

Speciation of Cp*Ir-octatungstate complexes in the reaction mixtures. To monitor coordination assembly of Cp*Ir-octatungstate species in the solution-state, we analyzed reaction mixtures of $[(\text{Cp}^*\text{IrCl})_2(\mu\text{-Cl})_2]$ and Na_2WO_4 in 1:10, 1:8, 1:6, 1:4, 1:2, and 1:1 molar ratios in deuterium oxide (D_2O) using ^1H NMR spectroscopy. ^1H NMR spectroscopy is a powerful tool to study solution-state speciation of diamagnetic organic-containing polyoxometalates because each species gives a characteristic ^1H NMR pattern that reflects the local symmetry of the organic unit.^{23, 38} Cp* shows a simple ^1H NMR spectrum comprising a singlet signal of its methyl's protons, and the coordination assembly of Cp*Ir-octatungstate complexes is conveniently scrutinized by tracking evolutions of the ^1H singlets of Cp* ligands. As described in the X-ray crystal structure section, all three Cp*Ir-octatungstate complexes have C_{2h} symmetry rendering each pair of

$\{\text{Cp}^*\text{Ir}\}^{2+}$, $\{\text{Cp}^*\text{Ir}(\text{OH}_2)\}^{2+}$, or $\{\text{Cp}^*\text{Ir}(\text{OH}_2)_2\}^{2+}$ units symmetrically equivalent and hence **1a**, **2a**, and **3a** are expected to show one, two, and three singlets in their ^1H NMR spectra, respectively.

^1H NMR spectra of the reaction mixtures (Figure 4a) show singlets between 1.40 and 1.60 ppm; the intense signal between 1.42 and 1.46 ppm arises from hydroxo-bridged Cp^*Ir dimers $[(\text{Cp}^*\text{Ir})_2(\mu\text{-OH})_3]^+$ which are the major hydrolysis product of $[(\text{Cp}^*\text{IrCl})_2(\mu\text{-Cl})_2]$ in aqueous solution (see equation 4). The singlets above 1.48 ppm are characteristic of Cp^*Ir -octatungstate complexes, and they are indicative of the formation of three distinct species on varying $[(\text{Cp}^*\text{IrCl})_2(\mu\text{-Cl})_2]/\text{Na}_2\text{WO}_4$ molar ratios. Mixtures with total iridium concentration less than tungsten concentration (traces i–iv) showed one singlet around 1.51–1.52 ppm corresponding to the formation of **1a**. When total iridium concentration equals tungsten concentration (1:2 mixture; trace v), a second singlet appears around 1.54 ppm; this signal is first observed as a minor component in the 1:4 $[(\text{Cp}^*\text{IrCl})_2(\mu\text{-Cl})_2]/\text{Na}_2\text{WO}_4$ mixture (trace iv). The appearance of two singlets in this region corroborates with the solid-state symmetry of **2a**. Finally, the third singlet around 1.56–1.57 ppm is observed in the 1:1 mixture (trace vi), and those three singlets are attributed to **3a**. This speciation study revealed the three Cp^*Ir -octatungstate complexes are formed through sequential coordination of $\{\text{Cp}^*\text{Ir}\}^{2+}$ cations onto an octatungstate anion until cationic **3a** complexes are produced, and their equilibria are controllable by adjusting molar ratios between $[(\text{Cp}^*\text{IrCl})_2(\mu\text{-Cl})_2]$ and Na_2WO_4 . Furthermore, the order in which $\{\text{Cp}^*\text{Ir}\}^{2+}$ binds to octatungstate may signal the basicity of octatungstate's oxygen atoms: bridging oxygen atoms of $\{\text{W}_3\text{O}_{12}(\mu_3\text{-OH})\}^{7-}$ > terminal oxygen atoms of $\{\text{W}_3\text{O}_{12}(\mu_3\text{-OH})\}^{7-}$ > terminal oxygen atoms of *cis*- $\{\text{WO}_2\}^{2+}$.

For comparison, ^1H NMR spectra of the solution of pure **1–3** are given in Figure 4b. Compounds **1**, **2**, and **3** have poor solubility in water, however, they readily dissolve in aqueous

potassium nitrate solution, methanol, and acetonitrile, respectively. Although **2** is highly soluble in methanol, its ^1H NMR spectrum was collected in a mixed d_3 -methanol (CD_3OH ; 0.02 mL) and D_2O (0.58 mL) to suppress the reaction of $\{\text{Cp}^*\text{Ir}\}^{2+}$ with methanol.³¹ The ^1H NMR spectra of **1** (singlets at 1.59 and 1.53 ppm; integration ratio 1:2) and **2** (singlets at 1.52, 1.50, 1.44; integration ratio 1:1:2) agree with their solid-state structure, indicating they dissolve intact in the respective solvents; the most upfield signals are of $[(\text{Cp}^*\text{Ir})_2(\mu\text{-OH})_3]^+$ (see Figure S5 for the ^1H NMR spectrum of pure $[(\text{Cp}^*\text{Ir})_2(\mu\text{-OH})_3](\text{OH})$ in D_2O). In addition, crystals of **2** (identified by single-crystal X-ray diffraction, see Figure S6) were deposited after standing the NMR solution overnight at 27 °C, further confirming the stability of **2a**. The ^1H NMR spectrum of **3** in d_3 -acetonitrile (CD_3CN) shows three major singlets at 1.84, 1.75, 1.69 ppm (marked with asterisks) with an integration ratio of 1:1:1 attributed to $[(\text{Cp}^*\text{Ir})_2\{\text{Cp}^*\text{Ir}(\text{OH}_2)\}_2\{\text{Cp}^*\text{Ir}(\text{OH}_2)_2\}_2\text{H}_2\text{W}_8\text{O}_{30}]^{2+}$ cations; several weaker signals were observed which arise, presumably, from acetonitrile-coordinated species $[\text{Cp}^*_6\text{Ir}_6\text{H}_2\text{W}_8\text{O}_{30}(\text{H}_2\text{O})_{6-x}(\text{CD}_3\text{CN})_x]^{2+}$ or small $\text{Cp}^*\text{Ir}\text{-CD}_3\text{CN}$ complexes produced from the partial decomposition of **3a**. Note the differences in Cp^* 's proton chemical shifts of pure **1–3** and Cp^*Ir -octatungstate complexes formed in the reaction mixtures are caused by dissolution conditions such as types of solvents and counterions (see Figure S5 for a comparison between ^1H NMR spectra of **1** in aqueous KNO_3 and KCl and **2** in $\text{CD}_3\text{OH}/\text{D}_2\text{O}$ and pure D_2O). Nevertheless, the ^1H NMR patterns of pure **1–3** and Cp^*Ir -octatungstate species in the reaction mixtures are comparable and are in good agreement with the respective solid-state structures.

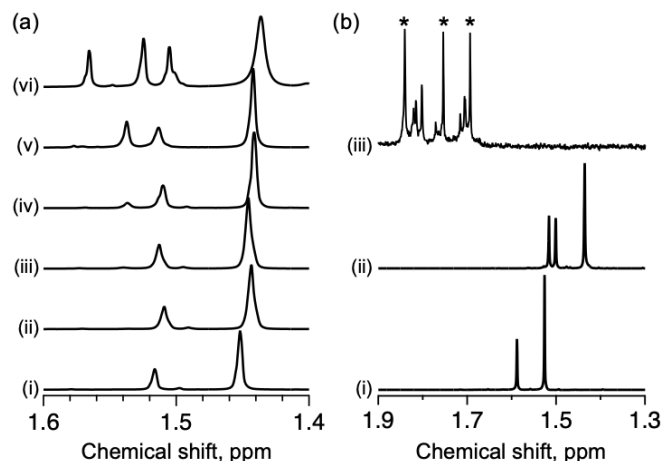


Figure 4. ^1H NMR spectra of (a) reaction mixtures containing $[(\text{Cp}^*\text{IrCl})_2(\mu\text{-Cl})_2]$ (0.025 mmol) with (i) 10, (ii) 8, (iii) 6, (iv) 4, (v) 2, and (vi) 1 equivalent of Na_2WO_4 in deuterium oxide (1.5 mL) and (b) solution of pure compounds (i) **1** in 1.0M $\text{KNO}_3/\text{D}_2\text{O}$, (ii) **2** in mixed $\text{CD}_3\text{OH}/\text{D}_2\text{O}$; **2** (c.a. 4 mg) was first dissolved in CD_3OH (0.02 mL) followed by addition of D_2O (0.58 mL), and (iii) **3** in CD_3CN ; singlets marked with an asterisk (*) are assigned to **3a**.

Structure-directing role of $\{\text{Cp}^*\text{Ir}\}^{2+}$ cations. We noticed a structural similarity between octatungstate $[\text{H}_2\text{W}_8\text{O}_{30}]^{10-}$ in **1–3** and paratungstate-B $[\text{H}_2\text{W}_{12}\text{O}_{42}]^{10-}$: both anions are -10 charged and comprise $\text{W}_3\text{O}_{12}(\mu_3\text{-OH})^{7-}$ building units (see Figure S7). Paratungstate-B is the dominant species in aqueous tungstate solution in a wide pH range and is isolable in the solid state.^{39, 40} The fact that octatungstate instead of paratungstate-B is formed in the presence of $\{\text{Cp}^*\text{Ir}\}^{2+}$ indicates a structure-directing property of $\{\text{Cp}^*\text{Ir}\}^{2+}$. To test this hypothesis, we carried out a reaction between $[(\text{Cp}^*\text{IrCl})_2(\mu\text{-Cl})_2]$ and methylammonium paratungstate-B $(\text{CH}_3\text{NH}_3)_{10}[\text{H}_2\text{W}_{12}\text{O}_{42}]$ —which has a high solubility in water⁴¹—as the tungsten source. The reaction produced an anionic Cp^*Ir -octatungstate complex containing methylamine ligands $[(\text{Cp}^*\text{Ir})_2\{\text{Cp}^*\text{Ir}(\text{NH}_2\text{CH}_3)\}_2\text{H}_2\text{W}_8\text{O}_{30}]^{2-}$ (**4a**) isolated as a methylammonium salt (**4**); **4a** was also

produced by adjusting pH of a 1:2 [(Cp*IrCl)₂(μ-Cl)₂]/Na₂WO₄ mixture to 7.5–8.0 by addition of aqueous methylamine solution from which it crystallized as Na[(Cp*Ir)₂(μ-OH)₃][(Cp*Ir)₂{Cp*Ir(NH₂CH₃)₂H₂W₈O₃₀] (**4'**). Anion **4a** has a similar structure (Figure 5a) to **2a** but with methylamine instead of water coordinating to each dangling {Cp*Ir}²⁺ units, and the Ir–N bond distance is 2.12 Å. The ¹H NMR spectra of [(Cp*IrCl)₂(μ-Cl)₂]/(CH₃NH₃)₁₀[H₂W₁₂O₄₂] reaction mixtures in 1:2, 1:1, and 2:1 molar ratios show **4a** complexes are the dominant species (Figure S8). Compound **4** slowly decomposes on dissolution in water (see ¹H NMR spectra in Figure S8), releasing [(Cp*Ir)₂(μ-OH)₃]⁺. This experiment supports {Cp*Ir}²⁺ direct self-assembly of octatungstate anions in an aqueous solution.

A space-filling model of **4a** (Figure S9) reveals methylamine molecules fit into the respective coordination site, and its methyl group weakly interacts with one of {W=O} terminal groups with a C⋯O separation at 3.27 Å. This feature suggests a possibility to tune the structure of Cp*Ir-octatungstate complexes by modifying the bulkiness of the organic amines. Thus, when pyridine instead of methylamine is introduced to a 1:10 [(Cp*IrCl)₂(μ-Cl)₂]/Na₂WO₄ mixture, **5** was produced. It comprises [(Cp*Ir)₂{Cp*Ir(NC₅H₅)₂H₂W₈O₃₀]²⁻ (**5a**) and [{Cp*Ir(NC₅H₅)₂(μ-OH)₂]²⁺; structure of the cationic complex has been reported.⁴² The larger size of pyridine compare to methylamine induces inversion of the orientation of the dangling {Cp*Ir(NC₅H₅)₂}²⁺ units so that the pyridine ligands are pointing away from the octatungstate core (Figure 5b), and Cp* ligands on the {Cp*Ir(NC₅H₅)₂}²⁺ units form weak interaction with terminal oxygen (O3) of octatungstate (*d* C⋯O = 3.38 and 3.51 Å).

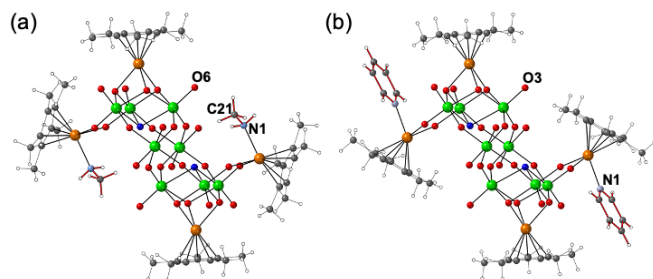


Figure 5. Ball-and-stick models of (a) **4a** in **4**; C21···O6 distance is 3.27 Å and (b) **5a**. Color scheme: green, W; orange, Ir; red, O; blue, protonated O (OH⁻); light blue, N; gray, C; white, H. Methylamine and pyridine molecules are emphasized by red bonds.

CONCLUSIONS

¹H NMR analyses of [(Cp*IrCl)₂(μ-Cl)₂]/Na₂WO₄ reaction mixtures confirm the formation of three kinds of Cp*Ir-octatungstate complexes identified as [(Cp*Ir)₂H₂W₈O₃₀]⁶⁻, [(Cp*Ir)₂{Cp*Ir(OH₂)₂}₂H₂W₈O₃₀]²⁻, and [(Cp*Ir)₂{Cp*Ir(OH₂)₂}₂Cp*Ir(OH₂)₂]₂H₂W₈O₃₀]²⁺ and their speciation is tunable by adjusting the molar ratios between [(Cp*IrCl)₂(μ-Cl)₂] and Na₂WO₄. The negative charge of the octatungstate anion is tuned by coordination with multiple {Cp*Ir}²⁺ units, and when six {Cp*Ir}²⁺ are coordinated the resulting complex becomes an organometallic polyoxocation. When (CH₃NH₃)₁₀[H₂W₁₂O₄₂] was used as the tungsten source, a methylamine-coordinated complex, [(Cp*Ir)₂{Cp*Ir(NH₂CH₃)₂]₂H₂W₈O₃₀]²⁻, is formed. Furthermore, the addition of pyridine to the 1:10 [(Cp*IrCl)₂(μ-Cl)₂]/Na₂WO₄ mixture produced [(Cp*Ir)₂{Cp*Ir(NC₅H₅)₂]₂H₂W₈O₃₀]²⁻ in which the orientation of {Cp*Ir(NC₅H₅)₂}²⁺ units is inverted with respect to the orientation of {Cp*Ir(NH₂CH₃)₂}²⁺ in the methylamine-coordinated complex. The octatungstate anions are formed regardless of the types of tungsten sources used in the synthesis, indicating a structure-directing property of {Cp*Ir}²⁺ cations. This study shows

anionic organometallic-polyoxometalate complexes possess high nucleophilicity, and hence, are potential building blocks for well-defined complex organometallic oxide clusters.

ASSOCIATED CONTENT

Supporting Information. List of Cp*Ir-polyoxometalate complexes and their synthetic conditions; crystallographic parameters of **1–5**; BVS values of W and O atoms in **1–5**; thermograms; structure of $[(\text{Cp}^*\text{Ir})_2(\mu\text{-OH})_3](\text{NO}_3)\cdot 6\text{H}_2\text{O}$; FTIR spectra; structure of $\text{Na}_2[(\text{Cp}^*\text{Ir})_2\{\text{Cp}^*\text{Ir}(\text{OH}_2)\}_2\text{H}_2\text{W}_8\text{O}_{30}] \cdot 26\text{H}_2\text{O}$; ^1H NMR spectra of $[(\text{Cp}^*\text{Ir})_2(\mu\text{-OH})_3](\text{OH})$, **1**, and **2**; unit cell parameters of **2** deposited from NMR $\text{CH}_3\text{OH}/\text{H}_2\text{O}$ mixture; structural comparison between $[\text{H}_2\text{W}_{12}\text{O}_{42}]^{10-}$ and $[\text{H}_2\text{W}_8\text{O}_{30}]^{10-}$ anions; ^1H NMR spectra of $[(\text{Cp}^*\text{IrCl})_2(\mu\text{-Cl})_2]/(\text{CH}_3\text{NH}_3)_{10}[\text{H}_2\text{W}_{12}\text{O}_{42}]$ mixtures and **4**; space-fill model of **4a**. The following files are available free of charge.

Supporting Information (PDF)

AUTHOR INFORMATION

Corresponding Author

*Email: sadakane09@hiroshima-u.ac.jp

Author Contributions

The manuscript was written through contributions of all authors. All authors have given approval to the final version of the manuscript.

Funding Sources

The New Energy and Industrial Technology and Development Organization (NEDO) Japan (Project JPNP20005), JSPS KAKENHI Grant-in-Aid for Transformative Research Area (A) “Supra-ceramics” (JP22H05144), JSPS Core-to-Core Program, and International Network on Polyoxometalate Science at Hiroshima University.

Notes

The authors declare no competing financial interest.

ACKNOWLEDGMENT

This work is commissioned by the New Energy and Industrial Technology and Development Organization (NEDO) and supported by JSPS KAKENHI Grant-in-Aid for Transformative Research Area (A) “Supra-ceramics” (JP22H05144), JSPS Core-to-Core Program, and International Network on Polyoxometalate Science at Hiroshima University. We acknowledge Ms. M. Kosaka and Mr. M. Kobayashi at the Division of Instrumental Analysis Okayama for performing CHN elemental analyses.

REFERENCES

- (1) Roesky, H. W.; Haiduc, I.; Hosmane, N. S. Organometallic oxides of main group and transition elements downsizing inorganic solids to small molecular fragments. *Chem. Rev.* **2003**, *103*, 2579-2595. DOI: 10.1021/cr020376q.
- (2) Isobe, K.; Yagasaki, A. Cubane-type clusters as potential models for inorganic solid surfaces. *Acc. Chem. Res.* **2002**, *26*, 524-529. DOI: 10.1021/ar00034a002.
- (3) Putaj, P.; Lefebvre, F. Polyoxometalates containing late transition and noble metal atoms. *Coord. Chem. Rev.* **2011**, *255*, 1642-1685. DOI: 10.1016/j.ccr.2011.01.030.
- (4) Artero, V.; Proust, A.; Herson, P.; Gouzerh, P. Interplay of Cubic Building Blocks in (η^6 -arene)Ruthenium-Containing Tungsten and Molybdenum Oxides. *Chem. Eur. J.* **2001**, *7*, 3901-3910. DOI: 10.1002/1521-3765(20010917)7:18<3901::Aid-chem3901>3.0.Co;2-3.

- (5) Villanneau, R.; Artero, V.; Laurencin, D.; Herson, P.; Proust, A.; Gouzerh, P. Organometallic polyoxometalates: synthesis and structural analysis of (η^6 -arene) ruthenium-containing polyoxomolybdates. *J. Mol. Struct.* **2003**, *656*, 67-77. DOI: 10.1016/s0022-2860(03)00356-9.
- (6) Hayashi, Y.; Müller, F.; Lin, Y.; Miller, S. M.; Anderson, O. P.; Finke, R. G. $2\text{CH}_3\text{CN} \subset (n\text{-Bu}_4\text{N})_2[\{\text{Ir}(1,5\text{-COD})\}_6\text{W}_4\text{O}_{16}] \cdot 2\text{CH}_3\text{CN}$: A Hybrid Inorganic–Organometallic, Flexible Cavity Host, Acetonitrile–Guest Complex Composed of a $[\text{W}_4\text{O}_4]^{n+}$ Tetrahedron and Six Polyoxoanion-Supported (1,5-COD) Ir^+ Organometallic Groups. *J. Am. Chem. Soc.* **1997**, *119*, 11401-11407. DOI: 10.1021/ja970336h.
- (7) Hayashi, S.; Shishido, T. High-Density Formation of Metal/Oxide Interfacial Catalytic Active Sites through Hybrid Clustering. *ACS Appl. Mater. Interfaces* **2021**, *13*, 22332-22340. DOI: 10.1021/acscami.1c02240.
- (8) Boujday, S.; Blanchard, J.; Villanneau, R.; Krafft, J. M.; Geantet, C.; Louis, C.; Breyse, M.; Proust, A. Polyoxomolybdate-stabilized Ru(0) nanoparticles deposited on mesoporous silica as catalysts for aromatic hydrogenation. *ChemPhysChem* **2007**, *8*, 2636-2642. DOI: 10.1002/cphc.200700533.
- (9) Ichikawa, M.; Pan, W.; Imada, Y.; Yamaguchi, M.; Isobe, K.; Shido, T. Surface-grafted metal oxide clusters and metal carbonyl clusters in zeolite micropores; XAFS/FTIR/TPD characterization and catalytic behavior. *J. Mol. Catal. A: Chem.* **1996**, *107*, 23-38. DOI: 10.1016/1381-1169(95)00226-x.
- (10) Do, Y.; You, X. Z.; Zhang, C.; Ozawa, Y.; Isobe, K. Trishomocubane-type methoxide cluster as a novel mediator in the extension of cube size in organometallic oxide clusters synthesis and structures of $[(\text{RhCp}^*)_2\text{Mo}_3\text{O}_9(\text{OMe})_4] \cdot \text{MeOH}$ and a linear quadruple cubane-type cluster $[(\text{RhCp}^*)_4\text{Mo}_6\text{O}_{22}] \cdot 4\text{CH}_2\text{Cl}_2$ ($\text{Cp}^* = \eta^5\text{-C}_5\text{Me}_5$). *J. Am. Chem. Soc.* **2002**, *113*, 5892-5893. DOI: 10.1021/ja00015a070.
- (11) Laurencin, D.; Thouvenot, R.; Boubekour, K.; Villain, F.; Villanneau, R.; Rohmer, M.-M.; Bénard, M.; Proust, A. Experimental and Computational Study of the Framework Fluxionality of Organometallic Derivatives of Polyoxometalates: Analysis of the Effect of the Metal and of the Solvent. *Organometallics* **2009**, *28*, 3140-3151. DOI: 10.1021/om8011568.
- (12) Laurencin, D.; Garcia Fidalgo, E.; Villanneau, R.; Villain, F.; Herson, P.; Pacifico, J.; Stoekli-Evans, H.; Benard, M.; Rohmer, M. M.; Suss-Fink, G.; Proust, A. Framework fluxionality of organometallic oxides: synthesis, crystal structure, EXAFS, and DFT studies on $[[\text{Ru}(\eta^6\text{-arene})_4\text{Mo}_4\text{O}_{16}]$ complexes. *Chem. Eur. J.* **2004**, *10*, 208-217. DOI: 10.1002/chem.200305396.
- (13) Abe, M.; Isobe, K.; Kida, K.; Nagasawa, A.; Yagasaki, A. Intramolecular rearrangements of cyclooctadienylrhodium(I) fragments supported on a vanadium oxide cluster as evidenced by dynamic ^{17}O NMR spectroscopy. *J. Cluster Sci.* **1994**, *5*, 565-571. DOI: 10.1007/bf01171386.
- (14) Akashi, H.; Isobe, K.; Ozawa, Y.; Yagasaki, A. β -Methallylrhodium(III) supported on a vanadium oxide cluster: Synthesis, structure, and reaction. *J. Cluster Sci.* **1991**, *2*, 291-296. DOI: 10.1007/bf00702958.
- (15) Mukhacheva, A. A.; Volcheck, V. V.; Sheven, D. G.; Yanshole, V. V.; Kompankov, N. B.; Haouas, M.; Abramov, P. A.; Sokolov, M. N. Coordination capacity of Keggin anions as polytopic ligands: case study of $[\text{VNb}_{12}\text{O}_{40}]^{15-}$. *Dalton Trans.* **2021**, *50*, 7078-7084. DOI: 10.1039/d1dt00765c.
- (16) Laurencin, D.; Villanneau, R.; Proust, A.; Brethon, A.; Arends, I. W. C. E.; Sheldon, R. A. Relationship between structure, fluxionality and racemization activity in organometallic derivatives of polyoxometalates. *Tetrahedron: Asymmetry* **2007**, *18*, 367-371. DOI: 10.1016/j.tetasy.2007.02.002.

- (17) Laurencin, D.; Thouvenot, R.; Boubekour, K.; Proust, A. Synthesis and reactivity of {Ru(*p*-cymene)}²⁺ derivatives of [Nb₆O₁₉]⁸⁻: a rational approach towards fluxional organometallic derivatives of polyoxometalates. *Dalton Trans.* **2007**, 1334-1345. DOI: 10.1039/b617390j.
- (18) Mougharbel, A. S.; Ahmedi, S.; Bhattacharya, S.; Rajan, A.; Kortz, U. Organorhodium(III)- and Iridium(III)-Substituted 20-Tungstobismuthates(III) and -Antimonates(III), [(MCp*)₂X₂W₂₀O₇₀]¹⁰⁻ (M = Rh^{III} and Ir^{III}, X = Bi^{III} and Sb^{III}). *ACS Omega* **2021**, *6*, 34494-34500. DOI: 10.1021/acsomega.1c04707.
- (19) Ikeda, K.; Mahyuddin, M. H.; Shiota, Y.; Staykov, A.; Matsumoto, T.; Ogo, S.; Yoshizawa, K. Computational Study on the Light-Induced Oxidation of Iridium-Aqua Complex to Iridium-Oxo Complex over WO₃(001) Surface. *Inorg. Chem.* **2020**, *59*, 415-422. DOI: 10.1021/acs.inorgchem.9b02704.
- (20) Gao, J.; Huang, X.; Cai, W.; Wang, Q.; Jia, C.; Liu, B. Rational Design of an Iridium-Tungsten Composite with an Iridium-Rich Surface for Acidic Water Oxidation. *ACS Appl. Mater. Interfaces* **2020**, *12*, 25991-26001. DOI: 10.1021/acsami.0c05906.
- (21) Singh, V.; Ma, P.; Drew, M. G. B.; Wang, J.; Niu, J. A comprehensive approach providing a new synthetic route for bimetallic electrocatalysts via isoPOMs [M/Rh(Cp*)₄W₈O₃₂] (M = Rh (1) and Ir (2)). *Dalton Trans.* **2018**, *47*, 13870-13879. DOI: 10.1039/c8dt03227k.
- (22) Abramov, P. A.; Vicent, C.; Kompankov, N. B.; Gushchin, A. L.; Sokolov, M. N. Coordination of {C₅Me₅Ir}²⁺ to [M₆O₁₉]⁸⁻ (M = Nb, Ta) - Analogies and Differences between Rh and Ir, Nb and Ta. *Eur. J. Inorg. Chem.* **2016**, *2016*, 154-160. DOI: 10.1002/ejic.201501051.
- (23) Kikuchi, M.; Ota, H.; López, X.; Nakaya, T.; Tsunoji, N.; Sano, T.; Sadakane, M. Reactivity of a (Benzene)Ruthenium(II) Cation on a Di-lacunary γ -Keggin-Type Silicotungstate and Synthesis of a Mono-(Benzene)Ruthenium(II)-Attached γ -Keggin-Type Silicotungstate. *Eur. J. Inorg. Chem.* **2018**, *2018*, 1778-1786. DOI: 10.1002/ejic.201701311.
- (24) Bi, L. H.; Chubarova, E. V.; Nsouli, N. H.; Dickman, M. H.; Kortz, U.; Keita, B.; Nadjo, L. Dilacunary decatungstates functionalized by organometallic ruthenium(II), [{Ru(C₆H₆)(H₂O)} {Ru(C₆H₆)}(γ -XW₁₀O₃₆)]⁴⁻ (X = Si, Ge). *Inorg. Chem.* **2006**, *45*, 8575-8583. DOI: 10.1021/ic0606835.
- (25) Bruker. *APEX3, SADABS, SAINT* **2016**.
- (26) Sheldrick, G. M. SHELXT - integrated space-group and crystal-structure determination. *Acta Crystallogr., Sect. A: Found. Adv.* **2015**, *71*, 3-8. DOI: 10.1107/S2053273314026370.
- (27) Sheldrick, G. M. Crystal structure refinement with SHELXL. *Acta Crystallogr., Sect. C: Struct. Chem.* **2015**, *71*, 3-8. DOI: 10.1107/S2053229614024218.
- (28) Hubschle, C. B.; Sheldrick, G. M.; Dittrich, B. ShelXle: a Qt graphical user interface for SHELXL. *J. Appl. Crystallogr.* **2011**, *44*, 1281-1284. DOI: 10.1107/S0021889811043202.
- (29) Spek, A. L. PLATON SQUEEZE: a tool for the calculation of the disordered solvent contribution to the calculated structure factors. *Acta Crystallogr., Sect. C: Struct. Chem.* **2015**, *71*, 9-18. DOI: 10.1107/S2053229614024929.
- (30) Brese, N. E.; O'Keeffe, M. Bond-valence parameters for solids. *Acta Crystallogr. Sect. B: Struct. Sci.* **1991**, *47*, 192-197. DOI: 10.1107/s0108768190011041.
- (31) Nutton, A.; Bailey, P. M.; Maitlis, P. M. Pentamethylcyclopentadienyl-rhodium and -iridium complexes. Part 29. Syntheses and X-ray structure determinations of [{Rh(C₅Me₅)}₂(OH)₃]OH·11H₂O and [{Ir(C₅Me₅)}₂(OH)₃]O₂CMe·14H₂O and related complexes. *J. Chem. Soc., Dalton Trans.* **1981**, 1997-2002. DOI: 10.1039/dt9810001997.

- (32) Niu, J.; Yang, L.; Zhao, J.; Ma, P.; Wang, J. Novel octatungstate-supported tricarbonyl metal derivatives: $\{[\text{H}_2\text{W}_8\text{O}_{30}][\text{M}(\text{CO})_3]_2\}^{8-}$ (M = Mn(I) and Re(I)). *Dalton Trans.* **2011**, *40*, 8298-8300. DOI: 10.1039/c1dt11042j.
- (33) Ogo, S.; Makihara, N.; Watanabe, Y. pH-Dependent Transfer Hydrogenation of Water-Soluble Carbonyl Compounds with $[\text{Cp}^*\text{Ir}^{\text{III}}(\text{H}_2\text{O})_3]^{2+}$ ($\text{Cp}^* = \eta^5\text{-C}_5\text{Me}_5$) as a Catalyst Precursor and HCOONa as a Hydrogen Donor in Water. *Organometallics* **1999**, *18*, 5470-5474. DOI: 10.1021/om9903689.
- (34) Adriaenssens, L.; Estarellas, C.; Vargas Jentzsch, A.; Martinez Belmonte, M.; Matile, S.; Ballester, P. Quantification of nitrate- π interactions and selective transport of nitrate using calix[4]pyrroles with two aromatic walls. *J. Am. Chem. Soc.* **2013**, *135*, 8324-8330. DOI: 10.1021/ja4021793.
- (35) Maheswari, P. U.; Modec, B.; Pevec, A.; Kozlevcar, B.; Massera, C.; Gamez, P.; Reedijk, J. Crystallographic evidence of nitrate- π interactions involving the electron-deficient 1,3,5-triazine ring. *Inorg. Chem.* **2006**, *45*, 6637-6645. DOI: 10.1021/ic060101j.
- (36) Wang, D. X.; Wang, M. X. Anion- π interactions: generality, binding strength, and structure. *J. Am. Chem. Soc.* **2013**, *135*, 892-897. DOI: 10.1021/ja310834w.
- (37) Schottel, B. L.; Chifotides, H. T.; Dunbar, K. R. Anion- π interactions. *Chem. Soc. Rev.* **2008**, *37*, 68-83. DOI: 10.1039/b614208g.
- (38) Sugiarto; Tagami, T.; Kawamoto, K.; Hayashi, Y. Synthesis of cationic molybdenum-cobalt heterometallic clusters protected against hydrolysis by macrocyclic triazacyclononane complexes. *Dalton Trans.* **2018**, *47*, 9657-9664. DOI: 10.1039/c8dt01226a.
- (39) Hastings, J. J.; Howarth, O. W. A 183W, 1H and 17O nuclear magnetic resonance study of aqueous isopolytungstates. *J. Chem. Soc., Dalton Trans.* **1992**. DOI: 10.1039/dt9920000209.
- (40) Gumerova, N. I.; Rompel, A. Polyoxometalates in solution: speciation under spotlight. *Chem. Soc. Rev.* **2020**, *49*, 7568-7601. DOI: 10.1039/d0cs00392a.
- (41) Candra Sukmana, N.; Sugiarto; Zhang, Z.; Sadakane, M. Structure and Thermal Transformations of Methylammonium Tungstate. *Z. Anorg. Allg. Chem.* **2021**, *647*, 1930-1937. DOI: 10.1002/zaac.202100219.
- (42) Lahoz, F. J.; Carmona, D.; Oro, L. A.; Lamata, M. P.; Puebla, M. P.; Foces-Foces, C.; Cano, F. h. Binuclear di- μ -hydroxo- and di- μ -methoxo-pentamethylcyclopentadienyl derivatives of rhodium and iridium with pyridine type ligands. Crystal structure of $[(\text{C}_5\text{Me}_5)\text{Rh}(\text{py})_2(\mu\text{-OH})_2][\text{ClO}_4]_2$ (py = pyridine). *J. Organomet. Chem.* **1986**, *316*, 221-227. DOI: 10.1016/0022-328x(86)82090-3.

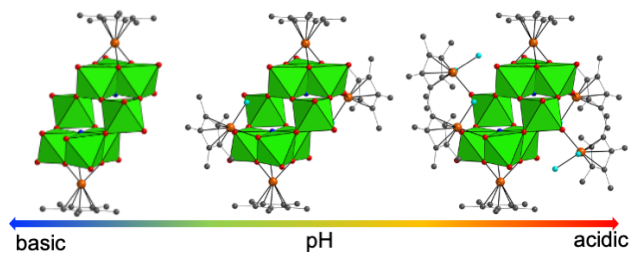
SYNOPSIS. The reaction of $[(\text{Cp}^*\text{IrCl})_2(\mu\text{-Cl})_2]$ and Na_2WO_4 in an aqueous solution produces three kinds of Cp^*Ir -octatungstate complexes and their speciation is tunable by adjusting molar ratios of the reactants and pH of the solution.

Graphical abstract.

$[\text{Cp}^*_2\text{Ir}_2\text{Cl}_4] + \text{Na}_2\text{WO}_4$ in aqueous solution

molar-ratio- and pH-dependent coordination assembly

$[\text{Cp}^*\text{Ir}^{2+}] < [\text{WO}_4^{2-}]$ $[\text{Cp}^*\text{Ir}^{2+}] = [\text{WO}_4^{2-}]$ $[\text{Cp}^*\text{Ir}^{2+}] > [\text{WO}_4^{2-}]$



Supporting Information

Molar-ratio-dependent coordination assembly of organoiridium(III)-octatungstate complexes in aqueous solution

*Sugiarto, Jun Shinogi, and Masahiro Sadakane**

Department of Applied Chemistry, Graduate School of Advanced Science and Engineering, Hiroshima University, 1-4-1 Kagamiyama, Higashi-Hiroshima 739-8527, Japan

*Email: sadakane09@hiroshima-u.ac.jp

Contents

Table S1. List of Cp*Ir-polyoxometalate complexes and their synthetic conditions	S2
Table S2. Crystallographic data for compounds 1–5	S3
Table S3. Bond valence sum (BVS) calculation results for 1–5	S4
Figure S1. Thermograms of 1–5	S5
Figure S2. Structure of [(Cp*Ir) ₂ (μ-OH) ₃](NO ₃)·6H ₂ O	S6
Figure S3. FTIR spectra of 1–5	S7
Figure S4. Structure of Na ₂ [(Cp*Ir) ₂ {Cp*Ir(OH ₂) ₂ } ₂ H ₂ W ₈ O ₃₀]·13H ₂ O	S8
Figure S5. ¹ H NMR spectra of [(Cp*Ir) ₂ (μ-OH) ₃](OH), 1 , and 2	S9
Figure S6. Unit cell parameters of 2 recrystallized from CH ₃ OH/H ₂ O	S10
Figure S7. Structural comparison between [H ₂ W ₁₂ O ₄₂] ¹⁰⁻ and [H ₂ W ₈ O ₃₀] ¹⁰⁻	S10
Figure S8. ¹ H NMR spectra of [(Cp*IrCl) ₂ (μ-Cl) ₂]/(CH ₃ NH ₃) ₁₀ [H ₂ W ₁₂ O ₄₂] mixture and 4	S11
Figure S9. Space-fill model of 4	S12
References	S12

Table S1. List of Cp*Ir-polyoxometalate complexes and their synthetic conditions

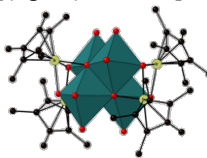
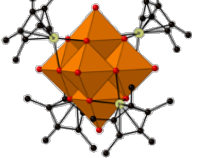
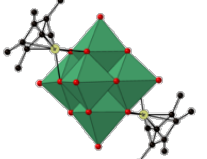
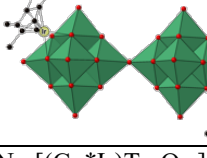
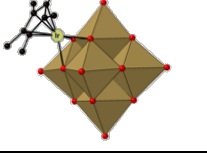
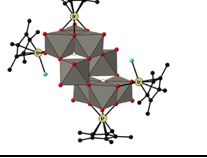
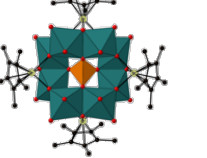
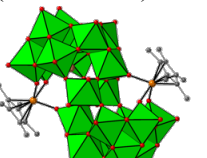
Structure	Synthetic conditions			Ref.
	POM source	Ir source	Solvent/condition	
$[(\text{Cp}^*\text{Ir})_4\text{Mo}_4\text{O}_{16}]$ 	$\text{Na}_2\text{MoO}_4 \cdot 2\text{H}_2\text{O}$ (8.3 mmol)	$[(\text{Cp}^*\text{Ir})_2(\mu\text{-Cl})_2]$ (0.8 mmol)	Water (8.0 mL) Reflux; 1 h	1
$[(\text{Cp}^*\text{Ir})_4\text{V}_6\text{O}_{19}]$ 	NaVO_3 (5.2 mmol)	$[(\text{Cp}^*\text{Ir})_2(\mu\text{-Cl})_2]$ (0.52 mmol)	Water (20.0 mL) Stir 30 min; r.t.	2, 3
$\text{Na}_4[(\text{Cp}^*\text{Ir})_2\text{Nb}_6\text{O}_{19}]$ 	$\text{Na}_7\text{H}[\text{Nb}_6\text{O}_{19}] \cdot 15\text{H}_2\text{O}$ (0.15 mmol)	$[(\text{Cp}^*\text{Ir})_2(\mu\text{-Cl})_2]$ (0.15 mmol)	Water (5.0 mL) Ethanol (0.1 mL) 60 °C; 48 h	4, 5
$\text{Na}_8\text{H}_2[(\text{Cp}^*\text{Ir})_2(\text{Nb}_6\text{O}_{18})_2\text{O}]$ 	$\text{Na}_7\text{H}[\text{Nb}_6\text{O}_{19}] \cdot 15\text{H}_2\text{O}$ (0.15 mmol)	$[(\text{Cp}^*\text{Ir})_2(\mu\text{-Cl})_2]$ (0.077 mmol)	Water (5.0 mL) Ethanol (0.1 mL) 60 °C; 48 h	
$\text{Na}_6[(\text{Cp}^*\text{Ir})\text{Ta}_6\text{O}_{19}]$ 	$\text{Na}_8[\text{Ta}_6\text{O}_{19}] \cdot 24.5\text{H}_2\text{O}$ (0.05 mmol)	$[(\text{Cp}^*\text{Ir})_2(\mu\text{-Cl})_2]$ (0.025 mmol)	Water (5.0 mL) Ethanol (0.1 mL) 60 °C; 48 h	
$\text{H}_4[(\text{Cp}^*\text{Ir})_4\text{W}_8\text{O}_{32}]$ 	$\text{Na}_2\text{WO}_4 \cdot 2\text{H}_2\text{O}$ (1.00 mmol)	$[(\text{Cp}^*\text{Ir})_2(\mu\text{-Cl})_2]$ (0.25 mmol)	Water (25 mL) 80 °C; 3 h	6
$\text{HNa}[(\text{Cp}^*\text{Ir})_4\text{PMo}_8\text{O}_{30}]$ 	$\text{Na}_2\text{MoO}_4 \cdot 2\text{H}_2\text{O}$ (1.00 mmol) 2 M H_3PO_4 pH 5	$[(\text{Cp}^*\text{Ir})_2(\mu\text{-Cl})_2]$ (0.50 mmol)	Water (25 mL) pH 6 80 °C; 3 h	7
$\text{Na}_{10}[(\text{Cp}^*\text{Ir})_2\text{X}_2\text{W}_{20}\text{O}_{70}]$ (X = Bi or Sb) 	$\text{Na}_{12}[\text{X}_2\text{W}_{22}\text{O}_{74}(\text{OH})_2]$ (0.014 mmol; X = Bi or Sb)	$[(\text{Cp}^*\text{Ir})_2(\mu\text{-Cl})_2]$ (0.014 mmol)	1 M CH_3COONa pH 6 70 °C; 30 min	8

Table S2. Crystallographic parameters for compounds 1–5. (*) Formula and formula weight based on X-ray diffraction results.

	1	2	3	4 (HKLF5 data set)	4'	5
Formula unit*	C ₃₀ H ₄₅ Ir ₃ Na ₂ O _{33.5} W ₄	C ₁₆₀ H ₂₄₀ Ir ₁₆ O _{114.4} W ₁₆	C ₆₀ H ₉₂ Ir ₆ N ₂ O ₅₆ W ₈	C ₄₂ H ₇₂ Ir ₄ N ₂ O ₄₈ W ₈	C ₆₂ H ₁₀₀ Ir ₆ N ₂ NaO ₆₉ W ₈	C ₈₀ H ₁₁₀ Ir ₆ N ₄ O ₄₄ W ₈
Formula weight* (g/mol)	2299.64	10010.71	4361.35	3612.61	4624.42	4455.71
Crystal system	Triclinic	Monoclinic	Triclinic	Monoclinic	Triclinic	Triclinic
Space group (number)	<i>P</i> $\bar{1}$ (2)	<i>C</i> 2/ <i>m</i> (12)	<i>P</i> $\bar{1}$ (2)	<i>P</i> 2 ₁ / <i>c</i>	<i>P</i> $\bar{1}$ (2)	<i>P</i> $\bar{1}$ (2)
a, Å	10.360(1)	22.656(1)	14.207(2)	12.470(1)	15.623(1)	14.137(1)
b, Å	16.355(1)	16.417(1)	14.819(2)	20.614(2)	16.719(1)	14.950(1)
c, Å	16.821(1)	21.661(2)	16.047(3)	17.441(2)	26.847(2)	16.407(1)
α, °	98.014(1)	90	104.272(2)	90	75.435(1)	109.857(1)
β, °	98.877(1)	114.591(1)	107.882(2)	106.327(1)	86.298(1)	106.836(1)
γ, °	90.524(1)	90	102.309(2)	90	63.127(1)	105.262(1)
V, Å ³	2787.0(4)	7326.1(9)	2959.1(8)	4302.6(8)	6044.3(8)	2858.7(3)
Z	2	1	1	2	2	1
D _{calc} (g/cm ³)	2.740	2.269	2.447	2.789	2.541	2.588
μ (mm ⁻¹)	15.457	13.553	14.532	16.889	14.247	15.038
Radiation	Mo Kα	Mo Kα	Mo Kα	Mo Kα	Mo Kα	Mo Kα
	(λ = 0.71073 Å)	(λ = 0.71073 Å)	(λ = 0.71073 Å)	(λ = 0.71073 Å)	(λ = 0.71073 Å)	(λ = 0.71073 Å)
Temperature (K)	123(2)	123(2)	123(2)	90(2)	123(2)	123(2)
F ₀₀₀	2084	4531	1968	3244	4206	2024
Θ range	1.258 to 27.103°	1.586 to 27.933°	1.415 to 27.621°	1.567 to 27.557°	1.410 to 26.373°	1.452 to 27.485°
Index ranges	-13 ≤ h ≤ 11 -20 ≤ k ≤ 19 -21 ≤ l ≤ 21	-29 ≤ h ≤ 29 -21 ≤ k ≤ 21 -28 ≤ l ≤ 24	-18 ≤ h ≤ 18 -19 ≤ k ≤ 19 -20 ≤ l ≤ 20	-16 ≤ h ≤ 15 0 ≤ k ≤ 26 0 ≤ l ≤ 22	-19 ≤ h ≤ 19 -20 ≤ k ≤ 20 -33 ≤ l ≤ 33	-18 ≤ h ≤ 9 -19 ≤ k ≤ 19 -21 ≤ l ≤ 20
No. of reflections collected	15839	32836	34795	9810	49131	16602
Unique reflections (<i>R</i> _{int})	11880 (0.0375)	9001 (0.0474)	13532 (0.0513)	9810	24413 (0.0587)	12601 (0.0196)
Data/restraints/parameters	11880/644/668	9001/470/574	13532/336/599	9810/616/430	24413/904/1334	12601/351/640
<i>R</i> indexes [<i>I</i> > 2σ(<i>I</i>)]	<i>R</i> ₁ ^a = 0.0444 <i>wR</i> ₂ ^b = 0.0919	<i>R</i> ₁ = 0.0342 <i>wR</i> ₂ = 0.0693	<i>R</i> ₁ = 0.0345 <i>wR</i> ₂ = 0.0674	<i>R</i> ₁ = 0.0431 <i>wR</i> ₂ = 0.0940	<i>R</i> ₁ = 0.0482 <i>wR</i> ₂ = 0.0910	<i>R</i> ₁ = 0.0319 <i>wR</i> ₂ = 0.0719
<i>R</i> indexes (all data)	<i>R</i> ₁ = 0.0610 <i>wR</i> ₂ = 0.0994	<i>R</i> ₁ = 0.0448 <i>wR</i> ₂ = 0.0827	<i>R</i> ₁ = 0.0516 <i>wR</i> ₂ = 0.0725	<i>R</i> ₁ = 0.0562 <i>wR</i> ₂ = 0.0992	<i>R</i> ₁ = 0.0772 <i>wR</i> ₂ = 0.1021	<i>R</i> ₁ = 0.0396 <i>wR</i> ₂ = 0.0748
G.O.F	1.004	1.043	0.0968	1.027	1.011	1.060
(Δ/σ) _{max}	0.001	0.002	0.001	0.001	0.002	0.001
Δρ _{max/min} (e Å ⁻³)	2.521/-2.638	2.115/-2.325	2.147/-1.836	2.218/-2.462	4.441/-2.718	2.905/-2.132
CCDC number	2218945	2218946	2218947	2226842	2218948	2218949

$$^a R_1 = \{\sum||F_o| - |F_c||\} / \{\sum|F_o|\}; \quad ^b wR_2 = [\sum w(F_o^2 - F_c^2) / \sum wF_o^2]^{1/2}$$

Table S3. BVS calculation results showing oxidation state of tungsten atoms and protonation state on oxygen atoms in **1–5**. Mono-protonated oxygen atoms (OH) are shown in red, whereas di-protonated oxygen atoms (H₂O) are shown in blue. Compound **4'** has two crystallographically independent molecules in the unit cell.

1	2	3	4	4'	5
W1 = 5.82	W1 = 5.92	W1 = 5.94	W1 = 5.91	W1 = 5.93	W5 = 5.95
W2 = 5.79	W2 = 5.87	W2 = 5.82	W2 = 5.98	W2 = 5.91	W6 = 6.03
W3 = 5.82	W3 = 5.87	W3 = 5.97	W3 = 5.89	W3 = 5.93	W7 = 5.83
W4 = 5.70	O1 = 1.57	W4 = 5.85	W4 = 5.95	W4 = 5.85	W8 = 6.03
O1 = 1.57	O2 = 1.79	O1 = 1.88	O1 = 1.57	O1 = 1.87	O16 = 1.71
O2 = 1.71	O3 = 1.22	O2 = 1.69	O2 = 1.87	O2 = 1.65	O17 = 1.91
O3 = 1.68	O4 = 1.74	O3 = 1.74	O3 = 1.58	O3 = 1.84	O18 = 1.61
O4 = 1.81	O5 = 1.84	O4 = 1.60	O4 = 1.56	O4 = 1.55	O19 = 1.79
O5 = 1.50	O6 = 1.57	O5 = 1.87	O5 = 1.75	O5 = 1.78	O20 = 1.70
O6 = 1.49	O7 = 1.98	O6 = 1.23	O6 = 1.63	O6 = 1.80	O21 = 1.67
O7 = 1.98	O8 = 1.60	O7 = 1.57	O7 = 1.88	O7 = 2.03	O22 = 1.85
O8 = 1.74	O9 = 1.84	O8 = 1.85	O8 = 1.94	O8 = 1.78	O23 = 2.00
O9 = 1.72	O10 = 0.38	O9 = 1.80	O9 = 2.03	O9 = 1.61	O24 = 1.71
O10 = 1.48		O10 = 2.00	O10 = 1.27	O10 = 1.49	O25 = 1.60
O11 = 1.52		O11 = 1.54	O11 = 1.99	O11 = 2.01	O26 = 1.52
O12 = 1.99		O12 = 1.48	O12 = 1.73	O12 = 1.20	O27 = 2.02
O13 = 1.54		O16 = 0.38	O13 = 1.77	O13 = 1.69	O28 = 1.21
O14 = 1.16		O17 = 0.36	O14 = 1.62	O14 = 1.55	O29 = 1.89
O15 = 1.50		O18 = 0.38	O15 = 1.59	O15 = 1.88	O30 = 1.69
bridging hydroxo groups of [(Cp*Ir) ₂ (μ-OH) ₃] ⁺ or [{Cp*Ir(C ₅ H ₅ N)} ₂ (μ-OH) ₂] ²⁺ counter cations					
O16 = 0.80	O1H = 0.98	-	-	-	O16 = 0.88
O17 = 0.85	O2H = 0.76				
O18 = 0.83	O3H = 0.79				

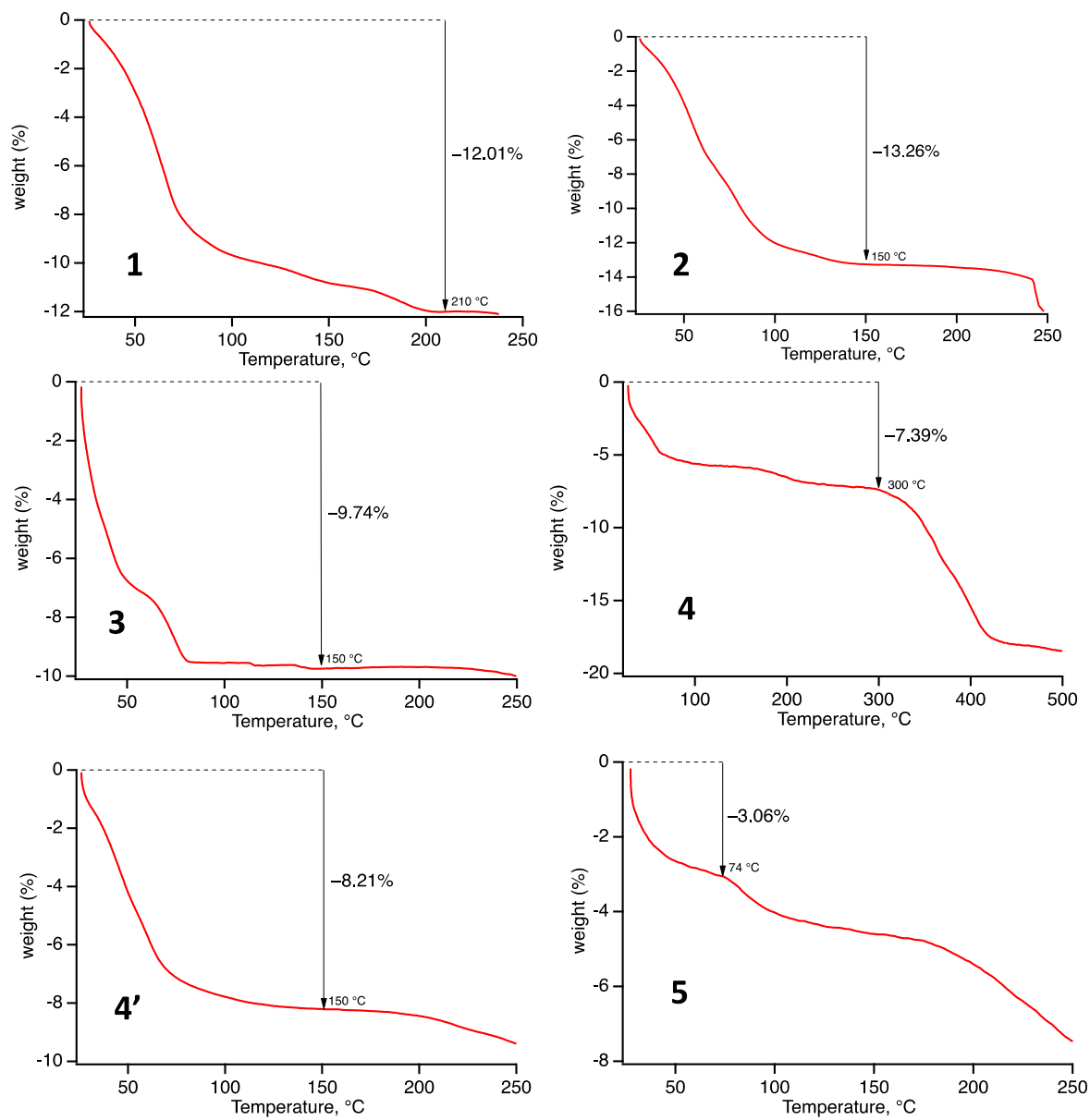
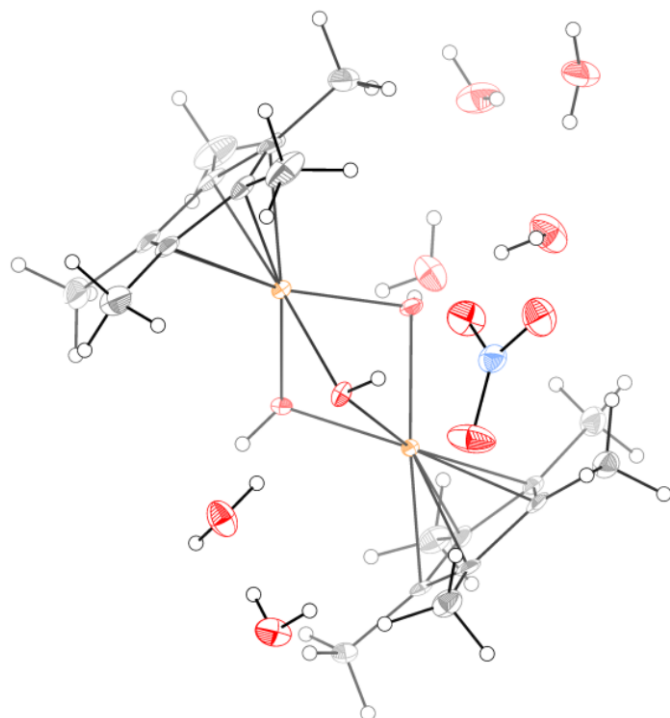


Figure S1. Thermograms of compounds 1–5.



$[(\text{Cp}^*\text{Ir})_2(\mu\text{-OH})_3](\text{NO}_3)\cdot 6\text{H}_2\text{O}$
 Monoclinic $P2_1/n$
 $a = 11.811(1) \text{ \AA}$
 $b = 14.132(1) \text{ \AA}$
 $c = 16.966(1) \text{ \AA}$
 $\beta = 90.520(1)^\circ$
 $V = 2831.8(4) \text{ \AA}^3$
 R_1 (all data) = 0.0263
 wR_2 (all data) = 0.0471
 GOF = 1.020
 $\Delta\rho_{\text{max/min}} = 0.879/-0.977 \text{ e \AA}^{-3}$

Figure S2. Thermal ellipsoid plot (at the 50% probability level) of $[(\text{Cp}^*\text{Ir})_2(\mu\text{-OH})_3](\text{NO}_3)\cdot 6\text{H}_2\text{O}$ and selected crystallographic parameters. Elem. Anal. calcd for $[(\text{Cp}^*\text{Ir})_2(\mu\text{-OH})_3](\text{NO}_3)\cdot 3\text{H}_2\text{O}$: C, 29.22; H, 4.79; N, 1.70. Found: C, 29.37; H, 4.51; N, 2.17. Color scheme: orange, Ir; red, O; blue, N; black, C. Hydrogen atoms are shown as white circles.

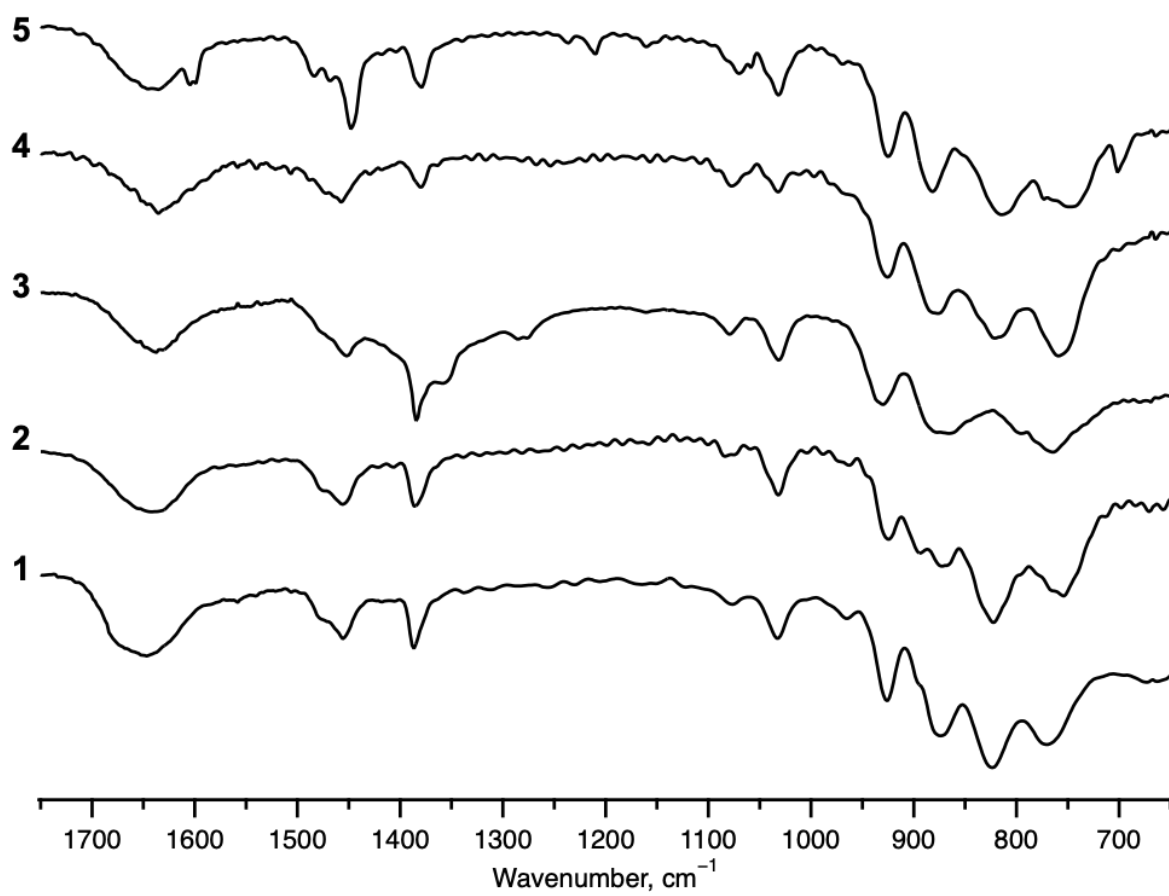


Figure S3. FTIR (in %transmittance) spectra of 1–5.

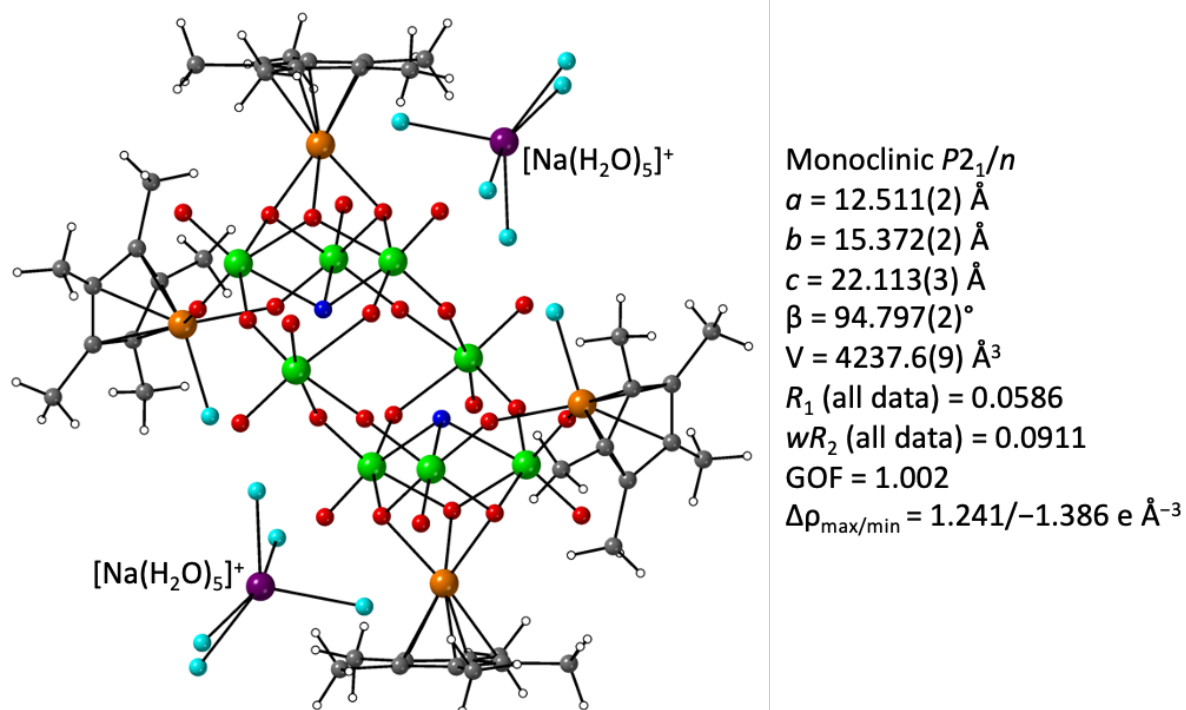


Figure S4. Structure of $\text{Na}_2[(\text{Cp}^*\text{Ir})_2\{\text{Cp}^*\text{Ir}(\text{OH}_2)\}_2\text{H}_2\text{W}_8\text{O}_{30}] \cdot 26\text{H}_2\text{O}$. Elem. Anal. calcd: C, 12.60; H, 3.13. Found: C, 12.53; H, 2.90. Color scheme: green, W; orange, Ir; purple, Na; red, O; blue, protonated O (OH^-); cyan, O of aquo ligands; gray, C; white, H.

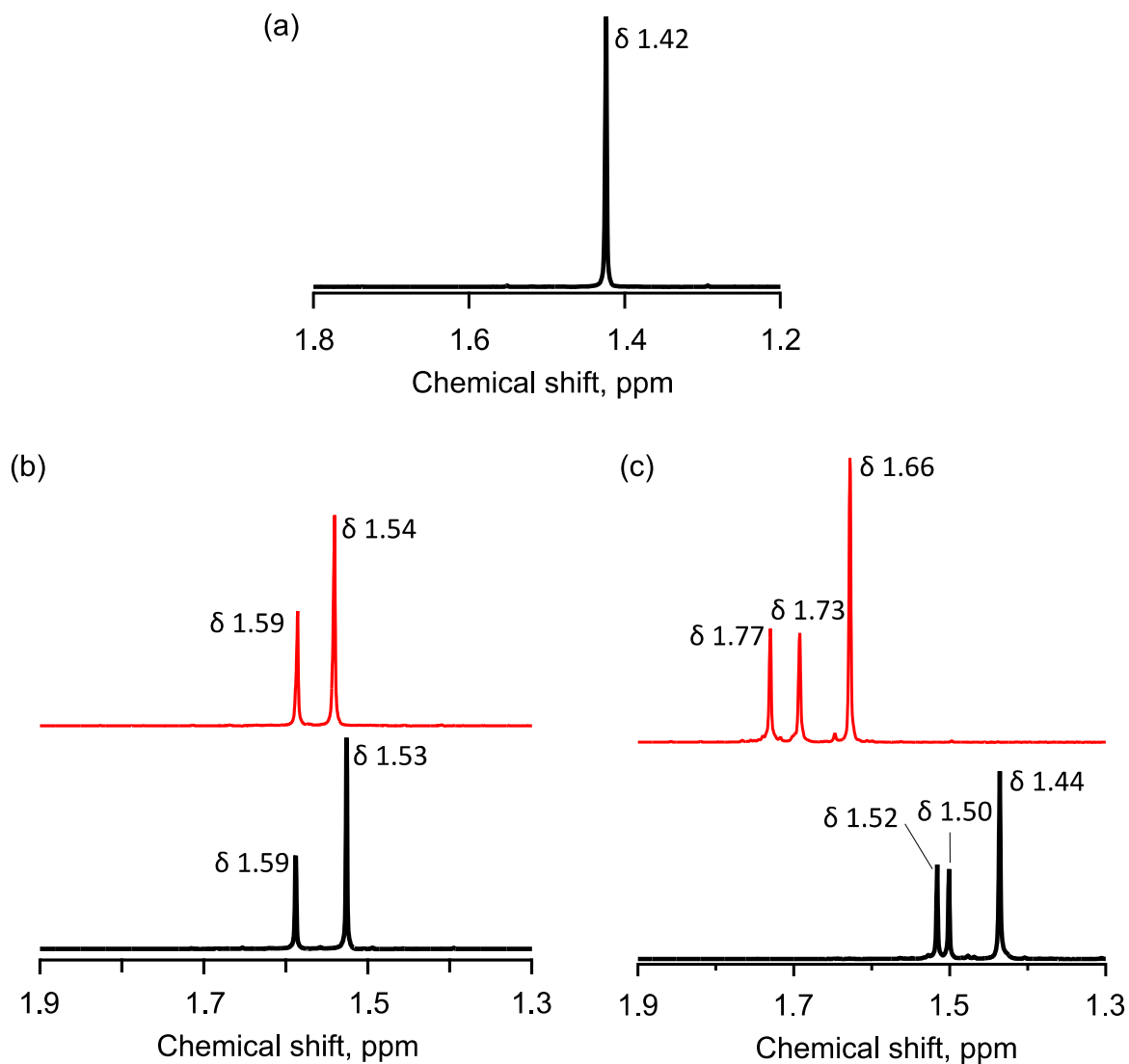
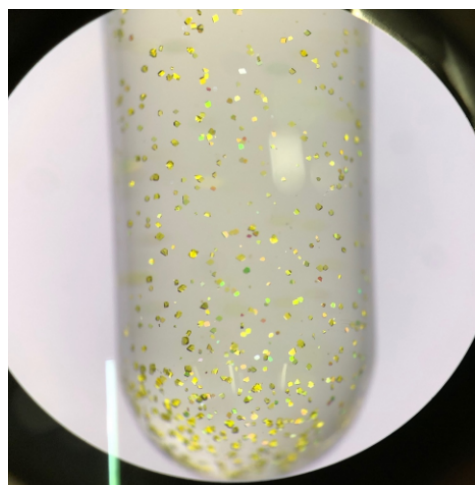


Figure S5. ^1H NMR spectra of (a) $[(\text{Cp}^*\text{Ir})_2(\mu\text{-OH})_3](\text{OH})$ in D_2O , (b) compound **1** in 1M $\text{KCl}/\text{D}_2\text{O}$ (red trace) and 1M $\text{KNO}_3/\text{D}_2\text{O}$ (black trace), and (c) compound **2** in CD_3OH (red trace) and mixed $\text{CD}_3\text{OH}/\text{D}_2\text{O}$ (black trace).



2 recrystallized from CH₃OH/H₂O Monoclinic *C2/m*
 $a = 22.633(2) \text{ \AA}$
 $b = 16.398(1) \text{ \AA}$
 $c = 21.645(3) \text{ \AA}$
 $\beta = 114.517(1)^\circ$
 $V = 7308.9(13) \text{ \AA}^3$

2 from [(Cp*Ir)₂(μ-Cl)₂]/Na₂WO₄ 1:2 Monoclinic *C2/m*
 $a = 22.656(1) \text{ \AA}$
 $b = 16.417(1) \text{ \AA}$
 $c = 21.661(2) \text{ \AA}$
 $\beta = 114.591(1)^\circ$
 $V = 7326.1(9) \text{ \AA}^3$

Figure S6. A photograph of crystals of **2** deposited from NMR solution. Their unit cell is similar to unit cell of **2** obtained from direct reaction between [(Cp*Ir)₂(μ-Cl)₂] and Na₂WO₄ (1:2 molar ratio).

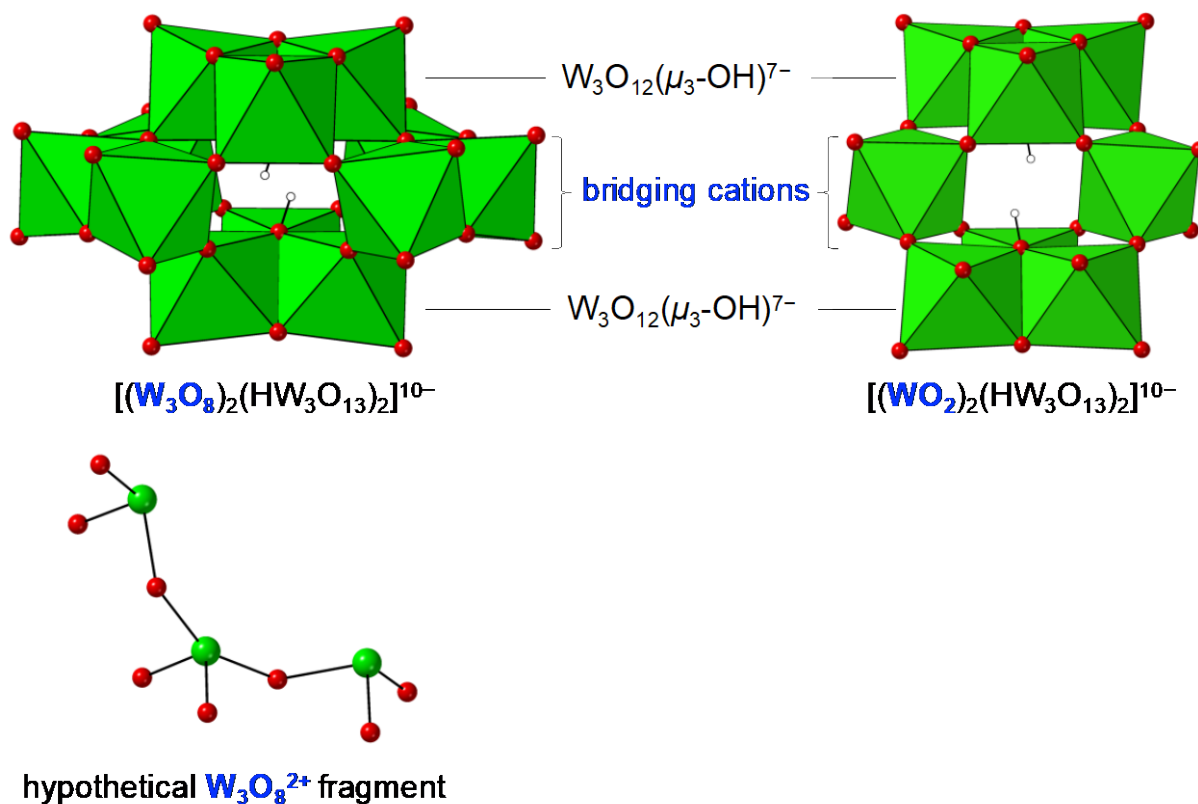


Figure S7. Structural comparison between paratungstate-B [H₂W₁₂O₄₂]¹⁰⁻ and octatungstate [H₂W₈O₃₀]¹⁰⁻. Tungsten atoms are located inside the green octahedra. Red spheres and white circles are oxygen and hydrogen atoms, respectively.

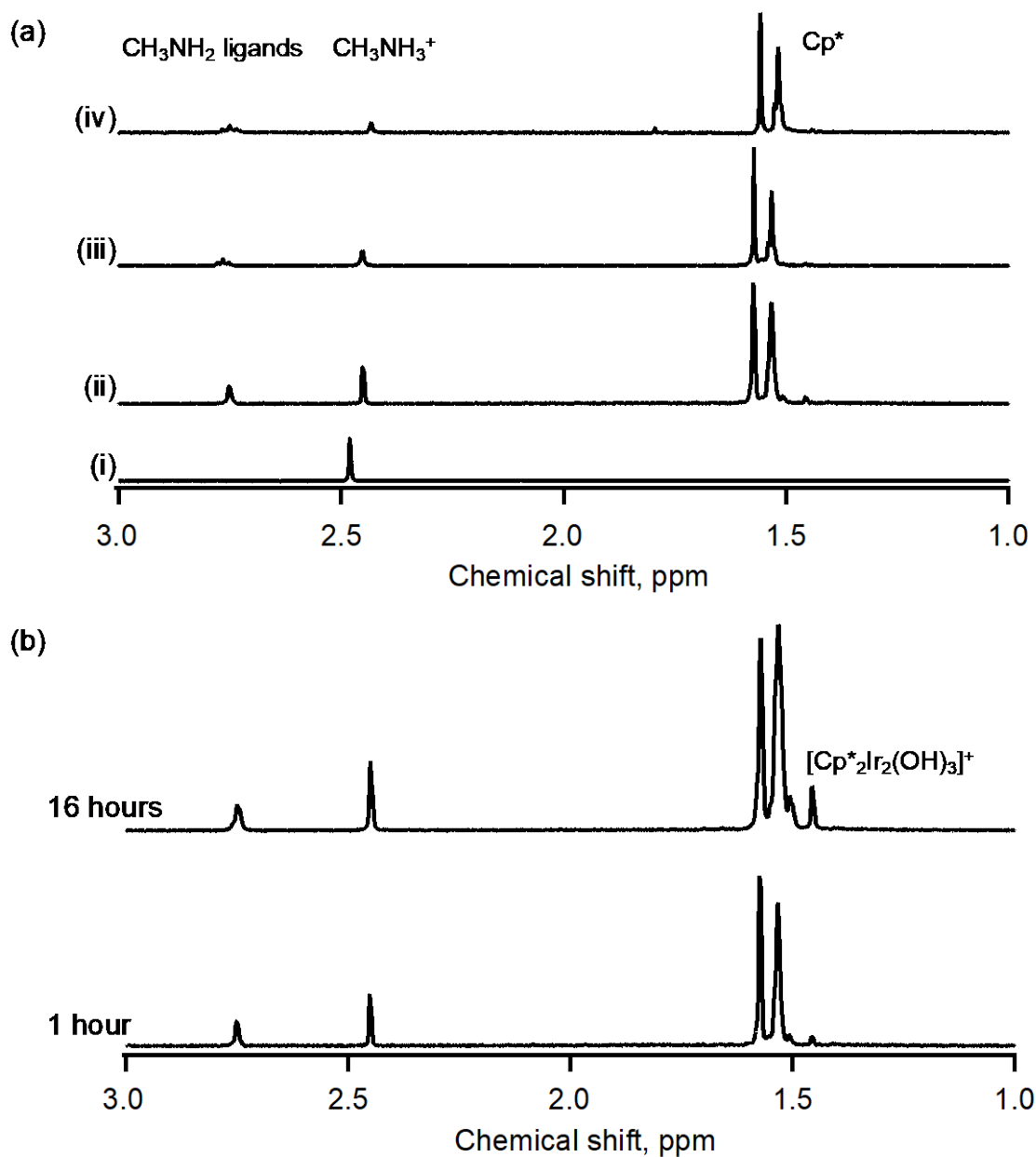


Figure S8. ^1H NMR spectra of (a) $(\text{CH}_3\text{NH}_3)_{10}[\text{H}_2\text{W}_{12}\text{O}_{42}]$ (trace i) and reaction mixtures of $[(\text{Cp}^*\text{Ir})_2(\mu\text{-Cl})_2]/(\text{CH}_3\text{NH}_3)_{10}[\text{H}_2\text{W}_{12}\text{O}_{42}]$ in 1:2 (trace ii), 1:1 (trace iii), and 2:1 (trace iv) molar ratios in deuterium oxide and (b) compound **4** aged for 1h and 16h.

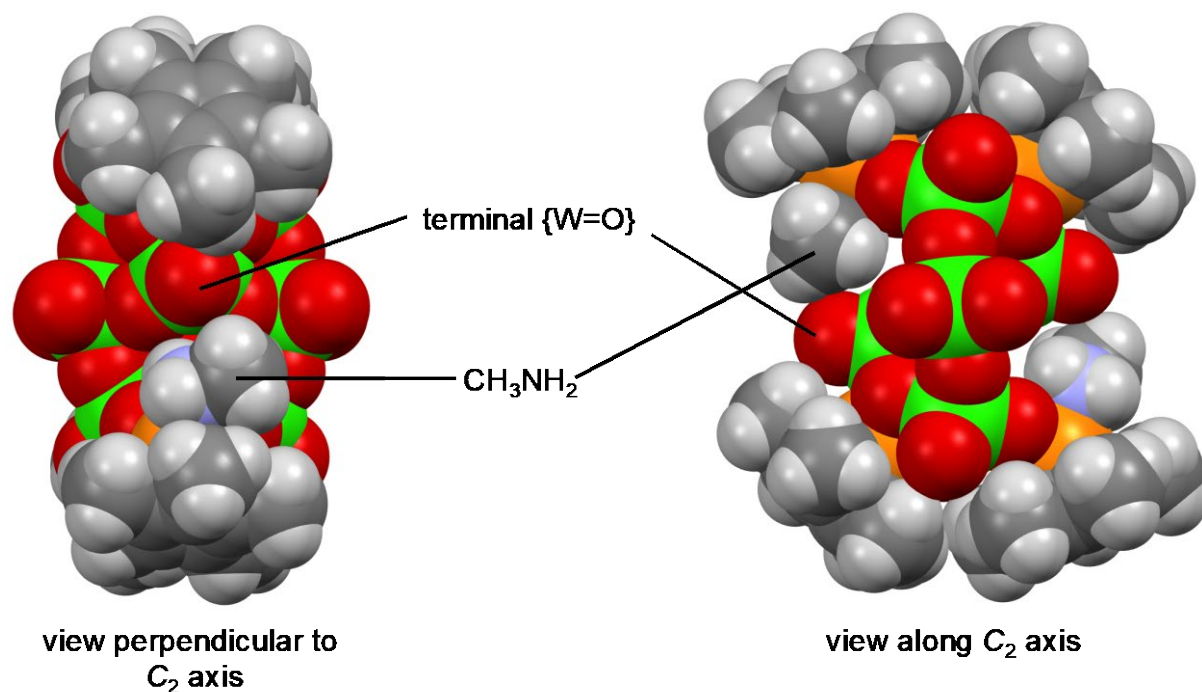


Figure S9. A space-fill model of **4a** showing steric environment around methylamine ligands. Color scheme: green, W; orange, Ir; red, O; blue, protonated O (OH⁻); light blue, N; gray, C; white, H.

References

- (1) Hayashi, Y.; Toriumi, K.; Isobe, K. Novel Triple Cubane-Type Organometallic Oxide Clusters: [MCp*MoO₄]₄·nH₂O (M = Rh and Ir; Cp* = C₅Me₅; n = 2 for Rh and 0 for Ir). *J. Am. Chem. Soc.* **1988**, *110*, 3666-3668. DOI: 10.1021/ja00219a056.
- (2) Hayashi, Y.; Ozawa, Y.; Isobe, K. The First “Vanadate Hexamer” Capped by Four Pentamethylcyclopentadienyl-rhodium or -iridium Groups. *Chem. Lett.* **1989**, *18*, 425-428. DOI: 10.1246/cl.1989.425.
- (3) Hayashi, Y.; Ozawa, Y.; Isobe, K. Site-selective oxygen exchange and substitution of organometallic groups in an amphiphilic quadruple-cubane-type cluster. Synthesis and molecular structure of [(MCp*)₄V₆O₁₉] (M = rhodium, iridium). *Inorg. Chem.* **1991**, *30*, 1025-1033. DOI: 10.1021/ic00005a028.
- (4) Abramov, P. A.; Vicent, C.; Kompankov, N. B.; Gushchin, A. L.; Sokolov, M. N. Coordination of {C₅Me₅Ir}²⁺ to [M₆O₁₉]⁸⁻ (M = Nb, Ta) - Analogies and Differences between Rh and Ir, Nb and Ta. *Eur. J. Inorg. Chem.* **2016**, *2016*, 154-160. DOI: 10.1002/ejic.201501051.
- (5) Abramov, P. A.; Sokolov, M. N.; Virovets, A. V.; Floquet, S.; Haouas, M.; Taulelle, F.; Cadot, E.; Vicent, C.; Fedin, V. P. Grafting {Cp*Rh}²⁺ on the surface of Nb and Ta Lindqvist-type POM. *Dalton Trans.* **2015**, *44*, 2234-2239. DOI: 10.1039/c4dt03339f.
- (6) Singh, V.; Ma, P.; Drew, M. G. B.; Wang, J.; Niu, J. A comprehensive approach providing a new synthetic route for bimetallic electrocatalysts via isoPOMs [M/Rh(Cp*)₄W₈O₃₂] (M = Rh (1) and Ir (2)). *Dalton Trans.* **2018**, *47*, 13870-13879. DOI: 10.1039/c8dt03227k.
- (7) Singh, V.; Ma, P.; Drew, M. G. B.; Niu, J.; Wang, J.; Jin, G. X. Heterooctamolybdate-Based Clusters H₃[(Cp*Rh)₄PMo₈O₃₂] and H₅[Na₂(Cp*Ir)₄PMo₈O₃₄] and Derived Hybrid Nanomaterials with Efficient Electrocatalytic Hydrogen Evolution Reaction Activity. *Inorg. Chem.* **2017**, *56*, 12520-12528. DOI: 10.1021/acs.inorgchem.7b01819.
- (8) Mougharbel, A. S.; Ahmedi, S.; Bhattacharya, S.; Rajan, A.; Kortz, U. Organorhodium(III)- and Iridium(III)-Substituted 20-Tungstobismuthates(III) and -Antimonates(III), [(MCp*)₂X₂W₂₀O₇₀]¹⁰⁻ (M = Rh^{III} and Ir^{III}; X = Bi^{III} and Sb^{III}). *ACS Omega* **2021**. DOI: 10.1021/acsomega.1c04707.